Article:
Wang, M., Ettelaie, R. orcid.org/0000-0002-6970-4650 and Sarkar, A. orcid.org/0000-0001-8677-5234 (2025) Surface adsorption of legume proteins upon tryptic hydrolysis: Theoretical and experimental study. Food Hydrocolloids. 111830. ISSN 0268-005X

https://doi.org/10.1016/j.foodhyd.2025.111830

Surface adsorption of legume proteins upon tryptic hydrolysis: Theoretical and experimental study

Mingxin Wang [1], Rammile Ettelaie [1*] and Anwesha Sarkar [1,2 *]

[1] Food Colloids and Bioprocessing Group, School of Food Science and Nutrition, University of Leeds, Leeds, LS2 9JT, UK

[2] National Alternative Protein Innovation Centre (NAPIC), UK

Corresponding authors:

*Prof. Anwesha Sarkar

E-mail address: A.Sarkar@leeds.ac.uk

*Dr. Rammile Ettelaie

E-mail address: r.ettelaie@leeds.ac.uk

Graphical Abstract

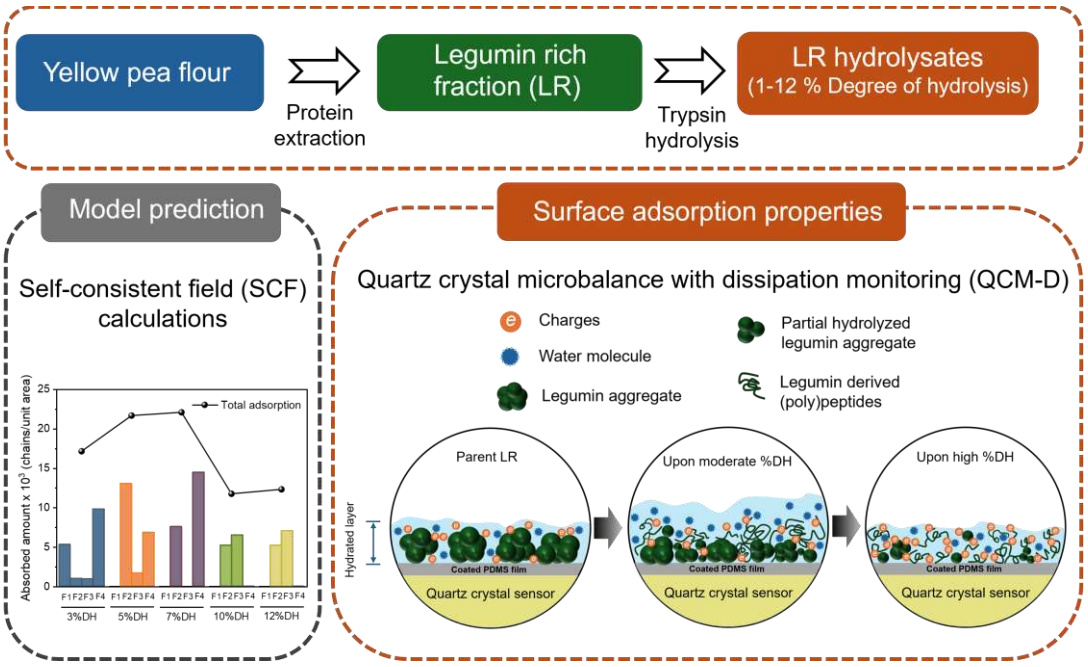

Highlights

- Combined theoretical and experimental study was performed on hydrolysis of legumin
- Moderate degree of hydrolysis (3–8 %) influenced surface adsorption positively
- Self-consistent field calculations showed increased fragment number per unit area upon 5–7 % degree of hydrolysis
- Tryptic hydrolysis decreased the hydrodynamic diameter of legumin aggregates
- Experimentally hydrated mass was higher with 3–8 %DH with high film viscoelasticity

Abstract

The aim of this study was to investigate the effects of enzymatic hydrolysis on surface adsorption of 11S legumin-rich fraction (LR), extracted from pea protein, using a combination of theoretical and experimental approaches. Experimentally, tryptic hydrolysates with 1-12 %degrees of hydrolysis (%DH) were produced at various enzyme to substrate ratios (1:50 to 1:1000 w/w), where moderate degrees of hydrolysis (up to

8 %DH) were found to be abundant in high molecular weight fractions. Tryptic hydrolysis reduced the particle size of LR aggregates from 270 nm to 119 nm and led to a higher degree of disordered structure as confirmed by circular dichroism (CD). Measurements using quartz crystal microbalance with dissipation monitoring (QCM-D), corroborated the observed enhancement in experimentally quantified surface hydrophobicity. Remarkably, we show that a narrow window of hydrolysis (3–8% DH) resulted in an increase in hydrated mass adsorbed on the hydrophobic surface as compared to unhydrolyzed legumin with a higher level of film viscoelasticity in the former. Theoretical Self-Consistent Field (SCF) calculations, involving the most abundant four fragments, demonstrated the relation between the nature of these hydrolysate fragments and surface adsorption. Moderate %DH (3-7%) resulted in a higher number of adsorbed fragments per unit hydrophobic surface area, supporting the QCM-D observations. However, this effect diminished at high %DHs. Findings from this study pinpoint the importance of a moderate degree of hydrolysis in improving surface adsorption behaviour of legume proteins, which might have implications for the design of sustainable plant protein-based formulations.

Key words: Pea protein; hydrolysates; enzymatic hydrolysis; Self-consistent field (SCF) theory; QCM-D; surface hydrophobicity

1 Introduction

As the growing population increasingly adopts veganism, there has been a subsequent rise in demand for plant-based foods (The Good Food Institute, 2023). When coupled with global sustainability concerns, this has led to significant research attention in plant-based protein food formulations in recent years. Plant proteins require considerably less energy to produce and result in fewer greenhouse gas emissions in comparison to their more

widely used animal counterparts (Poore & Nemecek, 2018). As a consequence, it is vital to explore palatable, nutritional and functional plant proteins to promote a sustainable dietary transition away from animal-derived proteins, with much current research devoted to understanding different functional performance of plant proteins in food systems (Jafarzadeh et al., 2024).

Pea proteins, part of the big family of legume proteins, are widely utilised due to their well-balanced amino acid profile, hypoallergenic properties and health benefits (Lu, He, Zhang, & Bing, 2020; Shanthakumar et al., 2022). However, pea protein isolates produced by conventional alkaline extraction with acid precipitation often exhibit a high degree of aggregation and poor solubility due to extensive denaturation caused by the harsh extraction process. Although there have been various emerging techniques providing mild extraction and fractionation conditions, the last drying step (either freeze drying or spray drying) can also be a source of further protein denaturation (Yang et al., 2022; Chen, Chiu, Feng, Maes, & Serventi, 2021). Consequently, pea protein extracts have been shown to display poor emulsifying properties (Morell, López-García, Hernando, & Quiles, 2023; Yang et al., 2023), high frictional performance (Kew, Holmes, Stieger, & Sarkar, 2021; Vlădescu et al., 2023; Zembyla et al., 2021) and inferior functional attributes. As a response, several modification methods have been developed and currently employed to improve plant protein techno-functionalities. These include high pressure treatment, ultrafiltration, fibrillization, micro-gelation to name a few (Kew et al., 2023; Nikbakht Nasrabadi, Sedaghat Doost, & Mezzenga, 2021).

Enzymatic hydrolysis is a “green” biochemical approach, that has been extensively used to modify protein structures through peptide bond cleavage, generating hydrolysates with lower molecular weight (Mw) and an altered hydrophobic-hydrophilic balance

(Vogelsang-O'Dwyer, Sahin, Arendt, & Zannini, 2022; Wouters, Rombouts, Fierens, Brijs, & Delcour, 2016). Several studies have reported improved interfacial, emulsifying and foaming properties of various legume proteins via enzymatic hydrolysis. For instance, Ghribi et al. (2015) reported a 40% increase in emulsifying ability and comparable emulsion stability of chickpea isolate as a result of 4 %DH, accompanied by increased solubility, flexibility and hydrophobicity. Arteaga et al. (2020) employed eleven different enzymes for pea protein hydrolysis, revealing a general improvement in emulsifying and foaming properties, especially with trypsin-produced hydrolysates exhibiting the most superior performance. One of the latest works on pepsin-induced lentil protein hydrolysates showed that 1.5 and 4.5 %DH led to a dense structured interfacial layer with stronger inter-plane interactions compared to native lentil protein, as seen in interfacial rheology measurements (Chutinara, Sagis, & Landman, 2024). However, the authors further observed inter-droplets flocculation in both sets of hydrolysate-stabilized emulsions, which was attributed to higher surface hydrophobicity of hydrolysates. Overall, most existing literature has focused on the effects of enzymatic hydrolysis on specific adsorption relevant functionalities (*i.e.* emulsifying and foaming capacities). Nevertheless, the fundamental understanding of enzymatic hydrolysis of proteins on surface adsorption behaviors, which can have a broader impact on colloidal properties as well as tribological performance has been rarely investigated (Wang, Ettelaie, & Sarkar, 2025).

Pea protein primarily consists of globulin (salt soluble) and albumin (water soluble), where each fraction exhibits its own unique structure and surface adsorption properties (Grossmann, 2024; Lesme, Kew, Bonnet, Sarkar, & Stellacci, 2024). For instance, legumin (11S, hexameric subunits with a Mw of 360-400 kDa) as one of the dominant storage proteins, can display lower solubility and inferior emulsifying capacity compared to vicilin

(7S, trimetric subunits with a Mw of 150-200 kDa) (Husband, Ferreira, Bu, Feyzi, & Ismail, 2024). It is also demonstrated that legumin shows the highest boundary friction as compared to albumin and vicilin (Lesme, Kew, Bonnet, Sarkar, & Stellacci, 2024). Hence, it is obvious that legumin as the most abundant fraction of pea protein has limited surface adsorption properties which may then influence the overall functional attributes of the protein, such as its emulsification, foaming and lubricity.

This study specifically aimed to extract legumin fraction from yellow pea and then examine how hydrolysis by trypsin may affect the physicochemical and surface adsorption properties of this otherwise poorly soluble protein. Experimentally, the extracted legumin-rich fraction (LR) was hydrolyzed by trypsin, a highly selective enzyme, to various degrees of hydrolysis (%DH) from 1% to 12%. We examined a wide range of physical attributes of such hydrolysates such as molecular weight, size, surface hydrophobicity and secondary structure as obtained by circular dichroism. This was followed by an examination of the effect of hydrolysis on surface adsorption behaviors, which were experimentally validated in a systematic manner for the first time, using quartz crystal microbalance with dissipation monitoring (QCM-D). Theoretically, to understand the enzyme-induced alteration in the resulting fragment profile and subsequent surface behaviors at a hydrophobic surface, mathematical calculations were conducted, followed by applying self-consistent field (SCF) calculations (Scheutjens & Fleer, 1979, 1980) to abundant legumin A hydrolysate fragments. The outcomes of this work can provide evidence for the potential of enzyme engineering of plant proteins to arrive at new plant protein-based ingredients with superior functionalities in future.

2 Materials and methods

2.1 Materials

Commercial yellow pea flour was purchased from Plant S (UK). Sodium chloride (NaCl) and trypsin from porcine pancreas (T4799) in the form of lyophilized powder were bought from Sigma Aldrich (Dorset, UK). All the chemicals for sodium dodecyl sulphate polyacrylamide gel electrophoresis (SDS-PAGE) (NuPAGE™, 4-12%, 1.0 mm X 12 well, Bis-Tris gradient gel; NuPAGE™ LDS Sample Buffer (4X); NuPAGE™ MES Running Buffer (10X); NuPAGE™ Sample Reducing Agent (10X); Novex™ Sharp Pre-stained Protein Standard) were purchased from Thermo Fisher Scientific (Loughborough, UK). The MilliQ water used for all experiments, which included sample extraction and dispersion) was retrieved from a Milli-Q apparatus (Millipore Corp., Bedford, MA, USA) with a resistivity of 18.2 MΩ·cm at 25 °C. Polydimethylsiloxane (PDMS) (base fluid and cross-linker (10:1 w/w)) was bought from Clearco (Sylgard 184, Dow Corning, Midland, MI, USA). Any other chemicals stated were analytical grade unless otherwise statement.

2.2 Extraction of pea legumin fraction

An aqueous procedure for extraction of legumin fraction from yellow pea flour was adopted from Rubio et al. (2014). The method is based on the difference of isoelectric points between legumin and vicilin fractions (4.6 and 5.5, respectively). Briefly, the yellow pea flour was dispersed in pH 8.0 MilliQ water with 0.5 M NaCl in a ratio of 1:10 under agitation for 2 h at room temperature (25 °C). The resultant dispersion was centrifuged (15 min, 5000 rpm, 4 °C), obtaining the supernatant. The supernatant was further adjusted to pH 4.5 by 1 M HCl under agitation for 1 h, followed by a second centrifugation step (15 min, 5000 rpm, 4 °C). The sediments were kept and redispersed in MilliQ water with a ratio of 1:4 w/v at pH 7. The resulting fraction was called legumin-rich fraction (LR) and was

158 dialyzed against MilliQ water using a 3.5 kDa cut-off membrane. The LR extracts were
159 frozen at -80 °C overnight and subsequently freeze-dried (Laconco freeze drier, Kansas,
160 USA) for 3 days. The final lyophilised LR powders were stored at -20 °C for future use.

161 2.3 Determination of total protein content

162 Nitrogen (N) content (%) of the lyophilised LR fraction was measured by combustion
163 method using Vario MICROCUBE elemental analyser (Elementar; Langenselbold,
164 Germany). The total protein content (%) was calculated by multiplying the nitrogen content
165 by 6.25 (Mariotti, Tomé, & Mirand, 2008).

166 2.4 Production of tryptic hydrolysates of pea legumin

167 Powder of LR fraction was dispersed in MilliQ water at a protein concentration of 2% w/v
168 under agitation at room temperature (25 °C) for 2 h and stored in fridge at 4 °C overnight
169 for sufficient protein hydration. In order to increase the effectiveness of enzymatic
170 hydrolysis, the protein suspension was treated with ultrasonication (300 W; 5 min) with an
171 ice bath to avoid sample overheating during the treatment (Ding et al., 2021). LR is referred
172 to ultrasonic treated LR fraction in the following usage. The LR dispersion was then
173 adjusted to pH 8.5 by using 1 M NaOH, and preheated to 37 °C, followed by adding trypsin
174 at various enzyme to substrate (E/S) ratios of 1:50, 1:100 and 1:1000 w/w to manipulate
175 the %DH. Specifically, a E/S ratio of 1:1000 w/w was chosen for reaching 1 and 3 %DH,
176 1:100 w/w was chosen for 5 and 8 %DH, and finally 1:50 w/w was applied to achieve 10
177 and 12 %DH based on our preliminary results. During the entire reaction, constant pH and
178 temperature were maintained by Metrohm 902 Titrando system (Metrohm Co., USA) and
179 water bath. The percentage degree of hydrolysis (%DH) was determined based on the pH-
180 stat method (Adler-Nissen, Eriksen, & Olsen, 1983). Hydrolysis by trypsin was terminated

by heating samples at 85 °C for 15 min in a shaking water bath once the target %DH was reached, which was indicated by the pH-stat system. Ater cooling to room temperature (~25 °C), the samples were adjusted to pH 7.0 prior to further analysis. Samples with different %DHs were prepared in duplicates. Samples produced with 1%, 3%, 5%, 8%, 10% and 12% DH were named henceforth as 1DH LRH, 3DH LRH, 5DH LRH, 8DH LRH, 10DH LRH, 12DH LRH, respectively.

2.5 Sodium dodecyl sulphate polyacrylamide gel electrophoresis (SDS-PAGE) analysis

SDS-PAGE analysis was carried out to examine the protein composition profile of the extracted LR and its hydrolysates (LRHs). Protein suspensions of 0.1 % (w/v) were mixed with LDS Sample Buffer (4X) and sample reducing agent (10X) or MilliQ water (for reducing and unreducing conditions, respectively), followed by protein denaturation in a water bath at 70 °C for 10 mins. Exactly, 10 μL of denatured protein samples and 5 μL of pre-stained protein molecular weight markers were loaded onto precast gels in an Invitrogen™ MiniGel Tank and submerged in MES running buffer (1X). After running the gel at a constant voltage 200 V for 30 mins, the gel was washed by MilliQ water and was then stained using Invitrogen™ SimplyBlue™ SafeStain overnight. The final image of the gel was taken by using a ChemiDoc™ XRS+ imaging system and Image Lab Software (Bio-Rad Laboratories, Richmond, CA, USA).

2.6 Particle size and zeta-potential

The particle size and zeta potential (ζ-potential) of LR and LRHs were conducted in a DTS1070 capillary cell using a ZetaSizer Ultra (Malvern Instruments Ltd., Worcestershire, UK) with an equilibration time of 120 s. The particle size was measured by dynamic light

scattering (DLS) with a backscattering angle of 173°, presented as the average hydrodynamic diameter (d_H) and polydispersity (PDI). The refractive indices (RI) of protein and aqueous phase were set as 1.45 and 1.33, respectively. All measurements were conducted in triplicates at a protein concentration of 0.01% w/v in phosphate buffer (PBS) at the neutral pH condition (pH 7.0), and at room temperature (25 °C).

2.7 Secondary structure

The secondary structure of LR and its hydrolysates (0.02% w/v protein dispersed in PBS solution) were investigated by Circular Dichroism (CD). Tests were conducted by scanning samples in a 1 mm path length quartz cuvettes under the Far-UV spectra between 190 and 260 nm, which was generated by Chirascan Plus (Applied PhotoPhysics Spectropolarimeter, Leatherhead, UK). A 2 nm bandwidth and 1 nm step size were used. Measurements for each sample were all conducted in triplicates at 25 °C, in addition to the PBS buffer solution as a blank.

2.8 Surface hydrophobicity

The relative surface hydrophobicity (H_0) of LR and LRHs was determined according to the method of Evangelho et al. (2017) with slight modification. Briefly, 1-anilino-8-naphthalenesulfonate (ANS) was used as a fluorescence probe, binding with the exposed hydrophobic regions of samples. Samples at 2% w/v protein levels were diluted in 10 mM PBS buffer at pH 7.0 to 0.002 % (w/v). Then 15 uL ANS (8 mM in 0.1 M PBS, pH 7.4) was added to the 3 mL of LR or LRHs. The systems were thoroughly mixed and left in the dark for 15 min before measurements. The fluorescence intensity of each sample was measured with a fixed excitation wavelength of 370 nm and an emission spectrum between

420 and 600 nm, using a FluoroMax spectrophotometer (HORIBA Scientific; USA). The slits of both excitation and emission were set at 5 nm.

2.9 Quartz crystal microbalance with dissipative monitoring (QCM-D)

The real time adsorption of LR and LRHs was measured by QCM-D (E4 system Q-Sense, Biolin Scientific, Sweden). Polydimethylsiloxane (PDMS) was used to coat the quartz crystal sensors to provide hydrophobic surfaces. To prepare the PDMS-coated sensors, 150 uL of PDMS solution (dissolved in toluene) was loaded on silicon sensors (QSX 303) and spin-coated by a spin coater with a 5000 rpm/s spinning speed for 60 min (Liamas, Connell, Zembyla, Ettelaie, & Sarkar, 2021). A vacuum oven was used afterwards for drying the coated layer at 80 °C overnight. Prior to QCM-D measurements, the newly coated sensors were cleaned by their immersion in toluene for 30 s, followed by a further 30 s immersion in isopropanol. This was then followed by 5 min immersion in MilliQ water. Sensors were then dried with nitrogen gas and left in the fume cupboard for at least 1 h for the solvent to evaporation before use.

All LR and LRHs samples were diluted into 10 mM pH 7.0 PBS buffer at a final protein concentration of 0.01% w/v, and were supplied into testing chambers by a peristaltic pump with a flow rate of 0.1 mL/min at 25 °C. A baseline correction procedure (reset to zero) was first implemented to eliminate any signal responses caused by external factors, such as the PDMS coating and PBS buffer. The experiment started with a 30-minute equilibration of the chambers using buffer flow, followed by introducing protein/hydrolysate solutions. Another rinsing step with PBS was conducted after around 2h sample adsorption until equilibrium with regards to both frequency and dissipation was achieved.

Data analysis was performed using Dfind software supplied by Biolin Scientific (Q-Sense, Sweden). Given the viscoelastic properties of protein films, data were fitted by using the Kevin-Voigt model (named as “Smartfit model” in the “Dfind” software), obtaining the hydrated mass of adsorbed protein layers. Two parameters are required as input to achieve the fitting, namely layer density (1100 g/L) and bulk liquid density (1006 g/L). The fitting equation employed can be found in Supplementary information equation (S2) and (S3). The 3rd, 5th, 7th, and 9th overtones were considered for data analysis, but only the 5th overtone was shown in the results here as a representative for both frequency and dissipation.

2.10 Statistical analysis

All results shown were performed in triplicate and plotted as a mean value with standard deviations. Significant differences between samples were determined by one-way ANOVA followed by Post Hoc multiple comparisons (Turkey’s test) using SPSS software (IBM, SPSS statistics) with 95% confidence level.

2.11 Probability calculation of possible LR fragments upon hydrolysis

Serials of equations were applied to obtain the probability of occurrence of possible fragments at a given %DH. As noted earlier, %DH is defined as the proportion of cleaved peptide bonds out of the total number of peptide bonds in the legumin A protein. Therefore, at a given %DH, the required number of broken bonds can be calculated as:

$$N_{\text{bro}} = (\%\text{DH})(N\text{p} - 1)/100 \quad (1)$$

where N_{p} is the total number of AA residues in the intact legumin A. Then, the probability of being cleaved for each susceptible peptide bond is required. In the case trypsin, it is well-established that it cleaves primarily at the carboxyl side of lysine and arginine (Gouseti

et al., 2023). However, even among these preferred cleavage sites, the actual probability of bond cleavage is not uniform. The cleavage efficiency can vary depending on the sequence context, such as the identity of adjacent amino acids, local secondary structure, and accessibility along the protein backbone (Deng, van der Veer, Sforza, Gruppen, & Wierenga, 2018). Unfortunately, such detailed knowledge regarding the differential susceptibility of each lysine and arginine carboxylic group is currently not available. Therefore, to simplify the system and make some progress in predicting the nature of fragments formed, we assumed an equal possibility for each trypsin-accessible bond to be hydrolysed, denoted as *P*. *P* can then be obtained by dividing N_{bro} by the total number of susceptible cleavage sites, denoted as N_s. By combining this with equation (1), *P* can be further expressed as:

$$P = \frac{\%DH \times (Np-1)}{100 \times Ns} \quad (2)$$

Therefore, for a potential fragment with the number of trypsin targeted sites of *i,* the probability of the occurrence of such fragment P_f was determined *via* the following equation:

$$P_f = P^2 \times (1-P)^{i-2} \quad (3)$$

where in order to form the fragment, 2 bonds at the terminus ends of the fragment must be cleaved, while the remaining *i*-2 bonds remain intact. Based on P_f, the relative volume fractions (V_f) of each possible fragments were calculated via equation (4) below to further represent the volume fraction contribution of each fragment to the system.

$$V_f = \frac{P_f \times N_f}{N_p} \quad (4)$$

where, N_f is the total AA residues of the generated fragment.

2.12 Self-consistent field (SCF) calculations

2.12.1 SCF theory

SCF calculations are well-established in the field of polymer physics. They can be used to offer information on the equilibrium properties of surface adsorbed protein layers. This calculation methodology has been widely adopted to analyse interactions mediated by the overlap of such adsorbed layers, providing meaningful insights on the likely emulsification as well as tribological performance (Dickinson, Horne, Pinfield, & Leermakers, 1997; Ettelaie, Akinshina, & Dickinson, 2008; Ettelaie, Khandelwal, & Wilkinson, 2014; Xu et al., 2020).

The implementation of the SCF calculations used in the present work is based on the scheme of Scheutjens-Fleer formulation of the theory (Scheutjens et al., 1979), which is defined on a 3D lattice grid. Specifically, the gap *L* between two approaching parallel surfaces is divided into a series of equal thickness layers parallel to the plates and further subdivided into equal-sized cubic cells (grid points). The thickness of each layer is given as the size of an individual monomer, a_0, which is taken to be the nominal size of each peptide bond ~0.3 nm. Given that the spatial distribution of AA monomers within the gap varies with the internal interactions among them (*i.e.* protein, solvent, ions), in SCF calculations, the most probable density profile for each specie in the gap is what is computed. To make the calculation practical, SCF theory invokes an approximation, considering the density profile with the lowest free energy (Ettelaie et al., 2008; Fleer, Stuart, Scheutjens, Cosgrove, & Vincent, 1993), *i.e.* the most probable one, as dominating the behaviour of the system. The essential question is now converted to one of finding the minimum value of the free energy as given by equation (S1) in supplementary information, which requires the knowledge of the fields $\psi_\alpha(r)$. This term captures the interactions

amongst species, and is crucial in determining the distribution of monomers (*i.e.* density profile) within the gap. $\psi_\alpha(r)$ is the sum of interaction potentials between type α AA residues with all other neighbouring monomers, ions or surfaces (if in contact with a surface), as given in equation (5). It encompasses the hard-core interactions (given by the term $\psi_h(r)$), long-ranged electrostatic interaction ($q_\alpha\psi_e(r)$) between the charged AA monomers and ions and short-ranged interactions ($\psi_{in}^{\alpha}(r)$) between each monomer (*e.g.* hydrophobic interaction, hydrogen bonding), specified using the Flory-Huggins interaction parameter $\chi_{\alpha\beta}$.

$$\psi_\alpha(r) = \psi_h(r) + q_\alpha\psi_{\ e}(r) + \psi_{in}^{\alpha}(r) \quad (5)$$

where the charge of species *α* is denoted as q_α. Yet, the fields themselves are in turn determined by how other residues are distributed around a monomer at any given point.

To this end, an iterative procedure is implemented whereby an initial rough guess of the set of interacting fields is chosen. These are used to calculate the density of each monomer according to a well-established procedure. This procedure will not be described here as it has already been discussed in numerous reviews and articles in the literature (Evers, Scheutjens, & Fleer, 1990; Scheutjens et al., 1979). From the resulting concentration profiles, a new set of interacting fields are then obtained in accordance with equation (2) and are employed for the next iteration of the calculations. The procedure is repeated until the field and profiles no longer substantially change from one iteration to the next and therefore become independent of further iterations.

2.12.2 Applied model

In the present study, the primary structure of legumin A with a composition of 517 AA residues derived from pea protein (P02857; sourced from online database UniProt) was

used for SCF calculations on fragments post-hydrolysis. Four most abundant fragments, predicted to be produced by hydrolysis, were considered in each case. Limiting the system to simultaneous presence of only these four fragments (out of a large set of such polypeptides) was mainly due to computer memory considerations, as well as the ease and speed of convergence here. However, in principle higher numbers can be dealt with if necessary. In other words, the input to the program consisted of the primary AA sequence information of those four fragments. Details of the fragments considered at different %DHs are explained later in the discussion section.

In the SCF model system, as implemented by us here, there are four types of components: protein, solvent, negatively and positively charged ions. All AA residues of legumin A are grouped into five categories, namely, polar, hydrophobic, positively charged, negatively charged residues according to their nature and chemical properties (Ettelaie et al., 2014), as detailed in **Table S2**. The interaction between monomers themselves, as well as those with solvent, ion and surface are expressed by a set of Flory-Huggins parameters $\{\chi\}$. The values used here were adopted from a previous work of Leermakers, Atkinson, Dickinson, and Horne (1996) and are listed in **Table 1**. Large positive value of $\chi_{\alpha\beta}$ indicates unfavourable interactions between type α and β monomers, whilst negative values represent favourable interactions. In this study, the distance between two surfaces can be changed from 2 to 80 layers (L = 80), giving a maximum separation distance of around 24 nm, assuming grid size a_0=0.3 nm. The surfaces were defined as hydrophobic, consistent with the PDMS-coated surface used in QCM-D analysis. Larger distances are again possible but require greater computational resources and involve slower convergence. The total bulk volume fraction of protein (Φ_{total}), *i.e.* when far away from the surface, is set to a low value of 1×10^{-6} in order to reflect the fact that post adsorption, most of the protein is

adsorbed on the surface, with very small amount actually remaining in the bulk solution. The volume fraction of those top four fragments generated after hydrolysis was determined (equation (6)) based on their relative volume fractions obtained in the previous section, and total volume fraction of intact protein prior to hydrolysis, Φ_t:

$$\Phi_f = V_f \times \Phi_t \quad (6)$$

The electrolyte volume fraction is fixed at a volume fraction of 0.001 (approximately equals to 10 mM NaCl) unless otherwise stated, and the environmental pH is 7.0. With the accomplishment of SCF calculations, the volume fraction of the polymer adjacent to the surface (density profile) can be obtained.

Table 1. The list of the Flory-Huggins interaction parameters ($\chi_{\alpha\beta}$) in the units of $k_B T$ given between different types of monomers, making up legumin A, solvent molecules and salt ions.

Monomer type [a]	0	1	2	3	4	5	6	7
0 - Solvent	0	1	0	0	0	0	-1	-1
1 - Hydrophobic residues	1	0	2.0	2.5	2.5	2.5	2.5	2.5
2 - Polar residues (non-charged)	0	2.0	0	0	0	0	0	0
3 - Positive residues	0	2.5	0	0	0	0	0	0
4 - Histidine (His)	0	2.5	0	0	0	0	0	0
5 - Negative residues	0	2.5	0	0	0	0	0	0
6 - Ion (+)	-1	2.5	0	0	0	0	0	0
7 - Ion (-)	-1	2.5	0	0	0	0	0	0
Hydrophobic surface	0	-2.0	0	0	0	0	0	0
pKa value	-	-	-	-	10	6.75	4.5	-

[a] The seven monomer types, labelled 0-7 in the first row, represent solvent, hydrophobic residues, polar residues, positively charged residues, Histidine, negatively charged residues, cationic ions, anionic ions, respectively.

[b] Negative values indicate attractive interactions, while positive values represent repulsive interactions.

Since the size of each considered fragment is not identical, it is important to gain information of their adsorbed amount (number of adsorbed chains/ unit area) besides their density profile. The adsorbed number surface density of a protein fragment is obtained as the integral of the excess amount of protein as compared to its bulk volume fraction, which is given as follows:

$$\Gamma^{\mathrm{exc}} = \frac{1}{N}\int_0^{\infty}(\phi(\mathrm{r}) - \phi_{\mathrm{bulk}})\mathrm{dr} \quad (2)$$

In the above equation, Γ is the number of adsorbed protein chains per unit area; N is the total number of AA residues of the protein fragment; $\Phi(\mathrm{r})$ is the volume fraction of that protein fragment at r, and Φ_{bulk} is the bulk protein volume fraction of the fragment far from the surface.

3 Results and discussion

3.1 The impacts of enzyme to substrate ratio (E/S) on experimentally validated degree of hydrolysis (%DH)

The effects of the enzyme to substrate ratio (E/S) on the time evolution of %DH was experimentally investigated as shown in **Figure 1**. The results indicated an enhanced level of hydrolysis at higher enzyme concentrations. The initial reaction rate, represented by the slope of %DH versus reaction time, showed a positive correlation with enzyme concentration (*i.e.* %DH increased to 1.9%, 4.0% and 6.2% after 20 min of hydrolysis at E/S ratios of 1:1000, 1:100 and 1:50, respectively). Furthermore, the maximum value of %DH achieved at 200 min substantially increased from 5.6 ± 0.4% to 10.9 ± 0.9% when the enzyme concentration increased by an order of magnitude from an E/S ratio of 1:1000 to 1:100 w/w. However, a further increase to 1:50 w/w resulted in only a minor additional

rise in the level of %DH at 200 min. This suggests that %DH at 200 min was approaching its theoretical maximum, as ultimately dictated by the limited number of peptide bonds susceptible to trypsin. Since this study specifically focused on trypsin hydrolysis, all C-terminal sides of lysine and arginine in protein backbone are considered susceptible to enzymatic cleavage (Gouseti et al., 2023). Such theoretical maximum %DH resulting from trypsin hydrolysis is therefore 13.4% (corresponding to 69 cleavage sites out of 516 peptide bonds), based on the AA composition of the Legumin A monomer (P02857; UniProt). The experimentally obtained maximum of 12.8% at the end of our experimental window (**Figure 1)** for the highest E/S ratio (1:50 w/w) was consistent with this theoretically predicted maximum value. Therefore, for subsequent analysis of the effects of %DH on LR properties, 12 %DH was selected as the upper limit for extensive hydrolysis in the following sections, as based on the maximum %DH obtainable from both theoretical predictions and our experimental results. Even the aforementioned maximum %DH can only ideally be achieved with a sufficiently long reaction time, as inactivation of enzyme and the product inhibition is always expected to occur during a very extended reaction time (Moreno & Cuadrado, 1993), as can be observed here for the case of E/S of 1:1000 w/w.

3.2 Physicochemical characterisation of the legumin-rich fraction upon tryptic hydrolysis

In this section, we investigated the physicochemical properties of hydrolysates derived from LR (with protein content of 84.4%) at varying %DH levels (*i.e.* 1, 3, 5, 8, 10, 12%).

3.2.1 SDS-PAGE

The protein composition of hydrolysed LR samples with different %DHs was analysed by SDS-PAGE under both reducing and non-reducing conditions, with untreated LR included

for comparison (**Figure 2a**). The control LR sample (lanes marked “LR” in both gels) exhibited the most intense legumin band, indicating that legumin is the primary composition of the LR extract. However, due to the similar properties of 11S legumin and 7S vicilin, contamination with the latter fraction cannot be completely discarded, as also previously reported (Bora, Brekke, & Powers, 1994; Lesme et al., 2024; Rubio et al., 2014).

Under reducing conditions, where disulfide bonds between the acidic and basic subunits are disassociated, LR was extensively composed of α-subunit (Mw of *ca.* 40 kDa) and β-subunit (Mw of *ca.* 20 kDa) (Meijers, Meinders, Vincken, & Wierenga, 2023), as depicted in **Figure 2a**. After hydrolysis, the α-subunit band completely disappeared, irrespective of the %DH level, while the β-subunit band remained visible. Additionally, a new intense band at Mw of ~33 kDa (designated as legumin-T (Klost & Drusch, 2019)) emerged, with its intensity gradually decreasing at 1-8 %DH before being fully digested at %DH >10%. This result can be explained by the unique structural characteristics of legumin. Several studies have previously reported that tryptic hydrolysis tends to start from the C-terminal regions of the α-subunit, which are located on the outer surface of legumin, whereas the more hydrophobic β-subunit is likely buried within the protein interior, making it less accessible to trypsin (Braudo et al., 2006; Plietz, Drescher, & Damaschun, 1987). As hydrolysis progresses, the unattached β-subunit could become exposed to trypsin, generating a large number of small fragments. This is evidenced by the intense bands observed below 5 kDa in the lanes corresponding to 10 and 12 %DH. (**Figure 2a**).

Under non-reducing conditions, it can be clearly observed that the main legumin band (~60 kDa) was digested resulting in lower Mw bands, consistent with the observation of Klost et al. (2019). The protein compositions of samples with increasing %DH from 1% to 8% showed no distinct differences. However, in hydrolysates with %DH above 8%, faint

450 bands in the high-Mw region and more intense bands below 8 kDa were observed,
451 highlighting extensive hydrolysis. Additionally, the intensity of protein residues at the
452 bottom of the gel wells gradually decreased as the reaction progressed, except for 1DH
453 LRH. This phenomenon suggests enhanced protein solubility induced by 3-12 %DH, which
454 could be attributed to the reduced size of polypeptides and the exposure of hydrophilic and
455 charged groups. A similar increase in solubility following hydrolysis has been widely
456 reported for various plant proteins (Shahbal, Jing, Bhandari, Dayananda, & Prakash, 2023).

457 **3.2.2 Particle size and *ζ*-potential upon hydrolysis**

458 **Figures 3a and 3b** show the averaged hydrodynamic diameter (d_H), polydispersity index
459 (PDI) and *ζ*-potential of LR and LRHs. In **Figure 3a**, a significant reduction in d_H can be
460 seen, from 267 nm to 119 nm, demonstrating the effectiveness of trypsin in breaking down
461 LR aggregates. This finding aligns with a previous study on another alternative protein *i.e.*
462 soy protein by Ding et al. (2021), where the substantial breakdown was attributed to
463 trypsin's high selectivity and ability to diffuse into the protein core. Notably, although the d_H
464 decreased with increasing %DH, PDI remained largely unchanged across most
465 hydrolysates, except for 1DH LRH. The size reduction influenced the visual appearance of
466 LR hydrolysates, as shown in **Figure 3b.** The turbidity of the samples decreased
467 significantly, becoming more transparent after 10 and 12 %DH. This change can be
468 expected with improved protein solubility with smaller fragments as observed in the
469 electrogram (**Figure 2a**), shifting from a dispersion to a solution.

470 As shown in **Figure 3b**, 1-5 %DH had a minor impact on the ζ-potential of
471 hydrolysates, which remained at approximately -22 mV at pH 7.0. However, with extended
472 reaction, a marked decrease to -30 mV was observed for 10 and 12 %DH LRH, which is

closely corroborated with the observation in our calculated net charge shown in **Table S1** (Supplementary information). This was likely due to the near-to-complete digestion of all fractions, resulting a large proportion of small fragments (as confirmed in SDS-PAGE profile, **Figure 2a**). These low Mw fragments exhibited low solvent mixing entropy and higher structural flexibility, facilitating conformational shifts that expose more hydrophilic or charged groups (Ding et al., 2023; Surówka, Żmudziński, & Surówka, 2004). Therefore, protein hydrolysates at 10 and 12 %DH may display stronger interactions with water molecule via increased electrostatic repulsions, also being evidenced with lower particle size (**Figure 3a**).

3.2.3 Surface hydrophobicity and secondary structure

The fluorescence spectra of the external ANS-probe and the Far-UV Circular Dichroism (CD) spectra for LR and LRHs are presented in **Figures 3c and 3d** to reflect their surface hydrophobicity (H_0) and secondary structure, respectively. These attributes are expected to play a remarkable role in protein surface adsorption by influencing both adsorption affinity and the mechanical properties of the resulting protein film (García-Moreno et al., 2021; Liamas, Connell, & Sarkar, 2023). In **Figure 3c**, 1DH LRH possessed the highest H_0 among all samples, and a following decrease in H_0 for 3-8 %DH was observed, although these values remained higher than that of LR. A similar trend was previously reported for pea protein isolate by Shuai et al. (2022). This overall increase in H_0 was attributed to the greater exposure of hydrophobic regions induced by enzyme cleavage. However, the subsequent decline after a certain %DH (1% in our case) might be due to the increased number of terminal hydrophilic groups, which likely promote a rebalance of hydrophobic-hydrophilic groups and possible reorganization of the disulfate group, thereby masking the hydrophobic patches again (Surówka et al., 2004; Zhang et al., 2023). As for those highly

497 hydrolysed samples (*i.e.* 10 and 12 %DH), their H_0 was remarkably lower than that of LR
498 and other LRHs (**Figure 3c**) possibly due to their highly fragmented nature. It is important
499 to note that a decrease in ANS-probe binding affinity could occur with small peptide
500 fragments containing fewer hydrophobic AAs or smaller hydrophobic regions (Latypov et
501 al., 2008), and this might contribute to an underestimation of fluorescence intensity (Chen,
502 Chen, Ren, & Zhao, 2011; Zhang & Romero, 2020).

503 **Figure 3d** shows the normalised CD spectra of LR and its LRHs, indicating significant
504 blue shifts of spectra after enzymatic treatments. As for LR, which exhibited typical α-helix
505 and β-sheet structure (Tahir, Jiang, & Ali, 2024), negative peaks in the 210-225 nm range,
506 as well as a positive peak at 192 nm were observed. After hydrolysis, the negative signal
507 above 210 nm lowered, excluding the 1DH LRH, which was indicative of decreased
508 proportion of α-helix and β-sheet structure (Hoffmann, Fano, & van de Weert, 2016). On
509 the other hand, as cases of 10 and 12 %DH LRH, the observed negative signal near 190
510 nm and lower signal above 210 nm demonstrated that they were predominantly disordered
511 (Venyaminov, Baikalov, Shen, Wu, & Yang, 1993). This was expected considering the near
512 complete digestion of all fractions and the dominant presence of small fragments as
513 evidenced in SDS-PAGE (**Figure 2a**).

514 ## 3.3 Impacts of %DH on surface adsorption behaviour of hydrolysates

515 The real-time surface adsorption behaviour of the unhydrolyzed LR and LRHs with
516 increasing %DHs was monitored by using quartz crystal microbalance with dissipation
517 monitoring (QCM-D). **Figures 4a and 4b** depicts the time-resolved frequence shift and
518 dissipation shift derived from protein adsorption (step P) and desorption (step B) occurring
519 on a PDMS-coated hydrophobic sensor. Surface adsorption using QCM-D has frequently

520 been correlated with tribology, mouth coating, as well as emulsification performance (Kew
521 et al., 2021; Stribițcaia et al., 2024; Yang, Zan, Li, Li, & Zhang, 2024). The changes in
522 frequency (Δf) and dissipation (ΔD) response are associated with changes in adsorbed
523 hydrated mass and film viscoelasticity, respectively. The raw data of Δf and ΔD attained
524 under multiple overtones (data not shown) was then fitted with Kevin-Voigt viscoelastic
525 model (details can be seen in Supplementary information) to obtain hydrated mass and
526 film thickness, as shown in **Figure 4c**.

527 After the injection of protein samples (step P), the detected *f* immediately decreased
528 (**Figure 4a**), with the corresponding *D* values simultaneously increased (**Figure 4b**),
529 indicating the adsorption of LR on given hydrophobic surface and building up of the film's
530 viscoelasticity. LRHs with 3~8 %DH displayed higher frequence gradient of ca. 50 Hz
531 (**Figure 4a**), implying enhanced mass adsorption, as compared to unhydrolyzed LR (Δf ~
532 42 Hz). Particularly, 8DH LRH exhibited the highest mass adsorption and film thickness
533 according to the quantitative estimation, with the value of ca. 23.8 mg/m^2 and 21.6 nm,
534 respectively, roughly 1.5-fold higher than that of LR (**Figure 4c**). This observation is in
535 close agreement with a previous study on whey protein hydrolysates, which employed the
536 same QCM-D technique and reported a highest *f* and *D* gradient for hydrolysates at 8%DH
537 (Tian et al., 2025). The higher surface hydrophobicity of hydrolysates and their relatively
538 large size, composed of a good number of hydrophobic AA residues, could corroborate
539 this improved surface adsorption. It is worthy emphasizing that the mass adsorption
540 measured using QCM-D does not only come from the adsorbate (*i.e.* protein) but
541 additionally the entrapped water within the hydrated layer of LR or LRHs. Therefore,
542 additional data fitting was conducted under two extreme conditions with layer density input
543 as 1006 and 1400 g/L considering the layer was pure hydrated (with negligible protein/

544 peptides) or purely protein/ peptides (almost no hydration), respectively. The observed
545 trend was similar as shown in **Figure 4c**, revealing the protein/hydrolysate adsorption at
546 moderate %DHs.

547 With further increase of %DH to 10% and 12%, the absolute value of both *f* and *D*
548 experienced a significant decrease, suggesting less adsorbed mass and a very rigid layer
549 formation (ΔD was close to 1 ppm) (see **Figures 4a and 4b**). The hydrated mass was ~12
550 mg/m^2 for 10 and 12 %DH hydrolysates, which was similar to those of LR and 1DH LRH
551 (**Figure 4c**). Additionally, a striking feature of high %DH hydrolysates illustrated in **Figure**
552 **4a** was a relatively high Δf change following the onset of the buffer rinsing-step B, which
553 revealed a high proportion of loosely bonded fragments that were washed out upon rinsing.
554 In other words, this most likely resulted from those small fragments with low surface binding
555 affinity at high %DH, that of similar behaviour was previously reported by Yang, Dai, Sun,
556 McClements, and Xu (2022) for small peptides (<5 kDa) derived from rice glutelin.

557 To obtain more information of the LR/LRHs adsorption kinetics and viscoelastic
558 properties of the formed films, plots of ΔD against Δf (so called *D-f* curve), independent of
559 time, is presented in **Figure 4d.** The slope of *D-f* curve was thought to be strongly related
560 to the viscoelasticity of the film, where a large value is indicative of a soft and hydrated film
561 (Teo et al., 2016), while a small slope value represents a rigid film with less water
562 entrapped (Kontturi, Tammelin, Johansson, & Stenius, 2008). The non-linear relation
563 between ΔD and Δf (**Figure 4d)** exhibiting two different slopes (K_1 and K_2) implied that the
564 characteristics of the adsorbed layers undergo a transition from viscoelastic to rather more
565 rigid as the layer builds up (Kim, Weber, Shin, Huang, & Liu, 2007). This could be explained
566 by the reorientation of adsorbed proteins and potential multilayer formation. To make better
567 qualitatively comparisons of the steady film viscoelasticity among LRHs, we selected the

568 value of $-\Delta D/\Delta f$ for each sample at their final equilibrium stage (*i.e.* after removing loosely
569 bonded proteins), as plotted in **Figure 4e**. It showed that layers of LRHs with 5 and 8 %DH
570 possessed comparable viscoelasticity, elucidating their highest degree of hydration ($-\Delta D/\Delta f$
571 ~0.12) compared to other samples (*i.e.* LR, 1%, 3%, 10% and 12% DH LRHs). Nonetheless,
572 beyond a certain %DH (*e.g.* above 10%), the adsorbed proteins tended to form more rigid
573 and less viscoelastic layers ($-\Delta D/\Delta f$ ~0.052), as a result of their highly disordered structure
574 and effective interfacial reorientation and packing. Overall, this suggests that
575 moderate %DHs might be beneficial for increasing the surface adsorption amount (higher
576 surface layer thickness) and the viscoelasticity of protein films, which might have
577 implication on improving emulsification and tribological performance, which warrants
578 further investigation.

579 ## 3.4 Predicted probability of generation of LR fragments

580 In order to gain molecular-level (or fragment-level) insights into the superior adsorption
581 performance of hydrolysates observed in the QCM-D analysis, mathematical calculations
582 were performed. The protein composition of the generated hydrolysate varies substantially
583 with different %DHs (Chen, Murray, & Ettelaie, 2023) and was subsequently predicted.

584 The volume fraction contributions of all possible fragments after 3, 5, 10 and 12 %DH
585 were calculated using equations (1)-(4). It is worth noting that, at the given %DH, the
586 resulting ensemble of generated fragments remains broadly identical regardless of the
587 reaction rate, which may be affected by differences in enzyme concentration and reaction
588 time. All possible resulting fragments were then classified into three groups based on their
589 chain length, namely, long, medium and short fragments. Casein, widely recognized for its
590 superior surface adsorption capability and known to be a good emulsifier, emulsion
591 stabilizer, as well as lubricating agent, consists of approximately 200 AA residues (Brown

et al., 2025; Dickinson, Pinfield, Horne, & Leermakers, 1997), hence we considered a medium length of 220 as an ideal fragment size. In addition, peptides with fewer than 20 AA residues are expected to lose their surface binding affinity, a property that has been specifically documented as lacking emulsifying ability (Girardet et al., 2000). Therefore, the thresholds for short and medium fragments were set as 20 and 220 residues, respectively, resulting in three fragment length-based populations: 0~20, 21~220 and 221~517. The distribution of each population as a function of %DHs is depicted in **Figure 5**. The volume fraction of long fragments massively decreased, reaching 0 by 3 %DH. As expected, the proportion of medium and short fragments increased accordingly. This finding corresponds to a previous prediction on averaged Mw made by Chen et al. (2023), which showed a dramatic rapid decline in Mw of fragments with the degree of hydrolysis, particularly in the low %DH range. Unlike the trends observed for short and long sized fragment populations, that of medium-sized fragments was non-monotonic, with volume fraction reaching a maximum at 3 %DH, followed by a decrease with further increases in the degree of hydrolysis. This relatively high proportion of medium-sized fragments following 3-9 %DH may partially explain our previous experimental conclusion that moderate %DH (3-8 %DH) enhance the surface adsorption performance of LR. This is consistent with the widely accepted notion that medium-sized chains exhibit superior surface activity and flexibility.

3.5 SCF calculations of surface adsorption of potential protein fragments post-hydrolysis

Once the potential protein fragments were predicted, the surface adsorption behavior of the hydrolysate system was investigated using SCF calculations, which accounted for the sequences of the fragments. Given the compositional complexity of the hydrolysate system

615 and the computational limitations of the SCF program in terms of the amount of computer
616 memory and computational run time, we simply considered the four fragments that are
617 most abundant for each %DH (*i.e.* the top four fragments based on their relative volume
618 fraction as given by (3)), for the subsequent SCF calculations. The list of selected
619 fragments under different %DHs is shown in **Table S3.** The sum of relative volume fraction
620 of these considered four fragments in each level of %DH is 0.036, 0.041, 0.064, 0.129,
621 0.186 for 3%, 5%, 7%, 10% and 12% DH, respectively.

622 In **Figure 6a**, the variation in the total adsorbed chains per unit area (a_0^2) is shown
623 as a function of %DH, indicating enhanced surface adsorption behaviour at 5 and 7 %DH,
624 which was corroborated our previous QCM-D observations (**Figure 4c**). For the 10 %DH
625 system, a lower level of adsorption was observed compared to more moderate %DHs. This
626 is not surprising considering that extensive hydrolysis may often result in less surface
627 affinity for the resulting chains (Ding, Zengin, Cheng, Wang, & Ettelaie, 2023). We also
628 assumed that this reduced adsorption was attributed to the higher charge density of
629 fragments at 10 %DH, with a theoretical net charge of -11.2 e (**Table S1**; see
630 supplementary information), thereby limiting further protein accumulation at surface due to
631 protein-protein electrostatic repulsion. This was similarly observed in experimental ζ-
632 potential value for hydrolysates with 10% and 12%DH. To further validate the effects of
633 charge, we conducted the same SCF calculations at a higher background electrolyte
634 volume fraction of 0.01 (~100 mM NaCl), where charge screening effects by salt should
635 occur. In this case, the results for 3-7 %DH remained similar with those obtained at low
636 salt condition. In contrast, for %DH=10, an increased number of adsorbed fragments was
637 found at higher salt concentrations where screening of charge is more prominent (**Figure**
638 **S2**). Nevertheless, with a further increase to 12 %DH, the four bulk dominant fragments

where the same ones as those at 10 %DH (**Table S3**), and the total chain adsorption was therefore comparable under both of these two levels of hydrolysis. This scenario is attributed to the lack of further susceptible bonds within the backbones of these fragments, due to the high selectivity of trypsin. Moreover, in all hydrolysate systems, co-adsorption of at least two constituent fragments were observed, further supporting the higher surface coverage as a result of more efficient adsorption by fragments of various sizes (Wang, et al., 2021).

Figure 6a shows that the most dominant fragment in the bulk solution (denoted as F1 in all cases) was not necessarily the one most abundant on the surface, implying the competitive adsorption between the fragments and highlighting the important role of protein AA primary sequence in determining the affinity of a polypeptide fragment for adsorption. The predicted configurations of the surface dominant fragments (F4, F2, F4, F3, F3 for 3, 5, 7, 10 and 12 %DH, respectively), as shown in **Figure 6b**, further illustrate this point. Interestingly, at 3-7 %DH, the dominant adsorbed fragment onto the hydrophobic surface were the same, despite the coexistence of various other fragments. This is somehow indicative of the superior surface affinity of the fragment Met ^{1} - Arg ^{23}. This fragment contains a relatively high number of hydrophobic AAs (see **Figure S1**, Supplementary information), enabling strong adsorption to the surface (Ding et al., 2023), along with its hydrophilic side extending away from the surface (~ 2nm; **Figure 6c**) into the bulk phase. As reported previously, this roughly “diblock-like” structure, is likely a desirable attribute for emulsion stabilisers and also to provide hydration lubrication as often seen in protein-polysaccharide system (Dickinson, 1999; Soltanahmadi, Murray, & Sarkar, 2022; Wooster & Augustin, 2007). When the hydrolysis reaction further progressed to 10 and then 12 %DH,

662 the fragment Leu ^{467} – Arg ^{490} emerged as the most dominant one at the surface, extending
663 with a similar distance ~2 nm away from the surface.

664 In **Figure 6c**, the total volume fraction (density profile) of the four-fragment
665 constituting mixtures adjacent to the given hydrophobic flat surface was illustrated,
666 providing complementary information on adsorption and interfacial film thickness. 3, 5 and
667 7 %DH led to a similar level of relative volume fractions closest to the surface ($\Phi \approx 0.5$).
668 When %DH increased to 10 and 12 %DH, a dramatic decrease in Φ was seen displaying
669 the value of 0.3. Additionally, the volume fraction decreased to zero at a distance of
670 approximately 2 nm (a reflection of surface layer thickness) across the %DH range of
671 5~12%, while it extended beyond 2.5 nm at 3 %DH. This observation can be expected,
672 given the longer length of Met ^{1} – Lys ^{60} under 3 %DH, which co-adsorbed with Met ^{1} - Arg
673 ^{23} (**Figure 6a**).

674 In summary, our theoretical work offers insightful interpretations at the molecular
675 level for legumin surface adsorption performance upon hydrolysis. First, fragments of
676 varying sizes generated by trypsin hydrolysis can co-adsorb, exerting synergistic effects
677 on adsorption amount and surface coverage. In addition, the AA composition of the
678 fragments and their resulting surface configurations significantly influence surface
679 adsorption, for example, 3-7 %DH generated a fragment with a superior AA sequence,
680 leading to a greater number of absorbed chains. These findings provide strong evidence
681 for our experimentally observed enhancement in surface adsorption behaviour of LR
682 following 3-8 %DH (as shown in **Figure 4c**). The potential mechanisms are visualised in
683 **Figure 7**.

684

4 Limitations

The limitations of this work include those inherent in the theoretical model applied, which is not able to capture the whole %DH range. Essentially, SCF calculations assume a flexible random coil type structure for proteins studied, where it is possible to take the linear primary sequence into consideration. At %0 and low %DH levels, most of the protein secondary structure remains unaltered in the protein, so that such assumptions of a coil like configuration may not be entirely accurate to perform SCF calculations. Nevertheless, most proteins will undergo unfolding during processing and thus the knowledge of results obtained from SCF calculations can still be helpful to understand the behavior of linear chains once undergone such processing-induced unfolding. We started with a %DH of 3%, where the generated fragments have reasonably short length (< 61 AAs) compared to the intact protein and could be assumed exhibiting a reasonable level of structural flexibility. Future investigations into advancing the SCF program with consideration of protein structure still require more attention. Experimentally, QCM-D analysis for surface adsorption can only record wet mass adsorption including water and protein molecules. Thus, the contribution of water or protein adsorbed is hard to distinguish. Nonetheless, the information on hydrated layers is still insightful to understand their real behavior when adsorbed on emulsion droplet surfaces or on mouth surfaces, where viscoelastic films they form can potentially lead to superior emulsion stability, smoothness and less astringency, respectively.

5 Conclusions

The goal of this present work was to fundamentally understand the effects of tryptic hydrolysis of legumin-rich fraction on surface adsorption properties through a combined approach of numerical SCF calculations and experimental measurements. In practical experiments, moderate hydrolysis (3-8 %DH) by trypsin effectively reduced the particle size and increased surface hydrophobicity of hydrolysates relative to the parent LR, while also imparting a more flexible structure. Surface adsorption analysis via QCM-D further revealed that the thickness and viscoelasticity of the surface protein layer derived from LRHs was highly responsive to %DHs, with 8DH LRH sample exhibiting the highest mass adsorption and hydration levels. This result potentially correlates with the enhanced bulk diffusion rate of hydrolysates, increased surface adsorption affinity and greater potential for reorientation upon adsorption. Theoretically, the probability of occurrence (and volume fraction contribution) of each possible fragments under varying %DHs was first mathematically calculated. Four most dominant fragments were then selected as the representative of the whole formed hydrolysates, and SCF was then applied to a mixture of these to gain insights into the surface adsorption behaviour of the fragmented proteins. It was seen that 5-7 %DH were beneficial for adsorption, demonstrating a higher number of fragments on the hydrophobic surface, further supporting experimentally validated QCM-D results. Additionally, within the polypeptide fragment mixture, we found clear evidence of competitive adsorption among compositionally different fragments, driven by differences in their primary sequence and surface configuration. Overall, this study provides detailed insights into possible ways of altering surface adsorption via tryptic hydrolysis of legume proteins, paving the way for future applications of enzyme-engineering of plant proteins for developing food formulations with optimised functional properties. Future work is necessary to validate these tailored surface functional properties of LRHs in specific

applications, such as emulsions and foams, or to understand how these properties translate into mouthfeel perception where often surface adsorption behaviour dominate the overall perception.

CRediT authorship contribution statement

Mingxin Wang: Conceptualization, Project administration, Methodology, Investigation, Formal Analysis, Data curation, Visualization; Writing- Original draft preparation, Writing-Reviewing & Editing, Rammile Ettelaie: Methodology, Conceptualization, Writing-Reviewing & Editing, Supervision; Anwesha Sarkar: Methodology, Conceptualization, Project administration; Writing- Reviewing & Editing, Supervision, Funding acquisition.

Acknowledgement

This work was funded by the UK National Alternative Protein Innovation Centre (NAPIC), which is an Innovation and Knowledge Centre funded by the Biotechnology and Biological Sciences Research Council (BBSRC) and Innovate UK (Grant Ref: BB/Z516119/1).

References

Adler-Nissen, J., Eriksen, S., & Olsen, H. S. (1983). Improvement of the functionality of vegetable proteins by controlled enzymatic hydrolysis. *Plant Foods for Human Nutrition, 32*(3), 411-423. https://doi.org/10.1007/BF01091198.

Bora, P. S., Brekke, C. J., & Powers, J. R. (1994). Heat Induced Gelation of Pea (Pisum sativum) Mixed Globulins, Vicilin and Legumin. *Journal of Food Science, 59*(3), 594-596. https://doi.org/10.1111/j.1365-2621.1994.tb05570.x.

Braudo, E. E., Danilenko, A. N., Guslyannikov, P. V., Kozhevnikov, G. O., Artykova, G. P., Lapteva, N. A., Vaintraub, I. A., Sironi, E., & Duranti, M. (2006). Comparative effects of limited tryptic hydrolysis on physicochemical and structural features of seed 11S globulins.

International Journal of Biological Macromolecules, 39(4), 174-178. https://doi.org/10.1016/j.ijbiomac.2005.12.006.

Brown, F., Soltanahmadi, S., Mackie, A. R., He, Q., Pfeifer, J., & Sarkar, A. (2025). Comparing frictional behaviour of plant and dairy proteins: Case study on high protein concentration. *Food Research International, 209*, 116322. https://doi.org/10.1016/j.foodres.2025.116322.

Chen, C., Murray, B. S., & Ettelaie, R. (2023). Surface adsorption properties of peptides produced by non-optimum pH pepsinolysis of proteins: A combined experimental and self-consistent-field calculation study. *Journal of Colloid and Interface Science, 652*, 405-417. https://doi.org/10.1016/j.jcis.2023.08.040.

Chen, L., Chen, J., Ren, J., & Zhao, M. (2011). Effects of Ultrasound Pretreatment on the Enzymatic Hydrolysis of Soy Protein Isolates and on the Emulsifying Properties of Hydrolysates. *Journal of Agricultural and Food Chemistry, 59*(6), 2600-2609. https://doi.org/10.1021/jf103771x.

Chen, W., Chiu, H. T., Feng, Z., Maes, E., & Serventi, L. (2021). Effect of Spray-Drying and Freeze-Drying on the Composition, Physical Properties, and Sensory Quality of Pea Processing Water (Liluva). Foods, 10(6), 1401. https://doi.org/10.3390/foods10061401.

Chutinara, C., Sagis, L. M. C., & Landman, J. (2024). Interfacial rheological properties of pepsin-hydrolyzed lentil protein isolate at oil-water interfaces. *Food Hydrocolloids, 155*, 110201. https://doi.org/10.1016/j.foodhyd.2024.110201.

Deng, Y., van der Veer, F., Sforza, S., Gruppen, H., & Wierenga, P. A. (2018). Towards predicting protein hydrolysis by bovine trypsin. *Process Biochemistry, 65*, 81-92. https://doi.org/10.1016/j.procbio.2017.11.006.

Dickinson, E. (1999). Caseins in emulsions: interfacial properties and interactions. *International Dairy Journal, 9*(3), 305-312. https://doi.org/10.1016/S0958-6946(99)00079-5.

Dickinson, E., J. Pinfield, V., S. Horne, D., & A. M. Leermakers, F. (1997). Self-consistent-field modelling of adsorbed casein Interaction between two protein-coated surfaces. *Journal of the Chemical Society, Faraday Transactions, 93*(9), 1785-1790. https://doi.org/10.1039/A608417F.

Dickinson, E., S. Horne, D., J. Pinfield, V., & A. M. Leermakers, F. (1997). Self-consistent-field modelling of casein adsorption Comparison of results for αs1-casein and β-casein. *Journal of the Chemical Society, Faraday Transactions, 93*(3), 425-432. https://doi.org/10.1039/a604864a.

Ding, Y., Chen, L., Shi, Y., Akhtar, M., Chen, J., & Ettelaie, R. (2021). Emulsifying and emulsion stabilizing properties of soy protein hydrolysates, covalently bonded to polysaccharides: The impact of enzyme choice and the degree of hydrolysis. *Food Hydrocolloids, 113*, 106519. https://doi.org/10.1016/j.foodhyd.2020.106519.

Ding, Y., Zengin, A., Cheng, W., Wang, L., & Ettelaie, R. (2023). Emulsifying properties of plant-derived polypeptide and their conjugates: a self-consistent-field calculation study of the impact of hydrolysis. *Soft Matter, 19*(38), 7443-7458.https://doi.org/10.1039/D3SM00855J.

Ettelaie, R., Akinshina, A., & Dickinson, E. (2008). Mixed protein–polysaccharide interfacial layers: a self consistent field calculation study. *Faraday Discussions, 139*(0), 161-178.https://doi.org/10.1039/B717199D.

Ettelaie, R., Khandelwal, N., & Wilkinson, R. (2014). Interactions between casein layers adsorbed on hydrophobic surfaces from self consistent field theory: κ-casein versus para-κ-casein. *Food Hydrocolloids, 34*, 236-246. https://doi.org/10.1016/j.foodhyd.2012.09.006.

Evangelho, J. A. d., Vanier, N. L., Pinto, V. Z., Berrios, J. J. D., Dias, A. R. G., & Zavareze, E. d. R. (2017). Black bean (Phaseolus vulgaris L.) protein hydrolysates: Physicochemical and functional properties. *Food Chemistry, 214*, 460-467. https://doi.org/10.1016/j.foodchem.2016.07.046.

Evers, O. A., Scheutjens, J. M. H. M., & Fleer, G. J. (1990). Statistical thermodynamics of block copolymer adsorption. 1. Formulation of the model and results for the adsorbed layer structure. *Macromolecules, 23*(25), 5221-5233. https://doi.org/10.1021/ma00227a009.

Fleer, G. J., Cohen Stuart, M. A., Scheutjens, J. M. H. M., Cosgrove, T., & Vincent, B. (1993). *Polymers at interfaces*: Chapman & Hall.

García-Moreno, P. J., Yang, J., Gregersen, S., Jones, N. C., Berton-Carabin, C. C., Sagis, L. M. C., Hoffmann, S. V., Marcatili, P., Overgaard, M. T., Hansen, E. B., & Jacobsen, C. (2021). The structure, viscoelasticity and charge of potato peptides adsorbed at the oil-water interface determine the physicochemical stability of fish oil-in-water emulsions. *Food Hydrocolloids, 115*, 106605. https://doi.org/10.1016/j.foodhyd.2021.106605.

García Arteaga, V., Apéstegui Guardia, M., Muranyi, I., Eisner, P., & Schweiggert-Weisz, U. (2020). Effect of enzymatic hydrolysis on molecular weight distribution, techno-functional properties and sensory perception of pea protein isolates. *Innovative Food Science & Emerging Technologies, 65*, 102449. https://doi.org/10.1016/j.ifset.2020.102449.

Girardet, J. M., Debomy, L., Courthaudon, J. L., Miclo, L., Humbert, G., & Gaillard, J. L. (2000). Viscoelastic Properties of Oil-Water Interfaces Covered by Bovine β-Casein Tryptic Peptides. *Journal of Dairy Science, 83*(11), 2410-2421. https://doi.org/10.3168/jds.S0022-0302(00)75130-7.

Gouseti, O., Larsen, M. E., Amin, A., Bakalis, S., Petersen, I. L., Lametsch, R., & Jensen, P. E. (2023). Applications of Enzyme Technology to Enhance Transition to Plant Proteins: A Review. Foods, 12(13), 2518. https://doi.org/10.3390/foods12132518.

Grossmann, L. (2024). Structural properties of pea proteins (Pisum sativum) for sustainable food matrices. *Critical Reviews in Food Science and Nutrition, 64*(23), 8346-8366. https://doi.org/10.1080/10408398.2023.2199338.

Hoffmann, S. V., Fano, M., & van de Weert, M. (2016). Circular Dichroism Spectroscopy for Structural Characterization of Proteins. In A. Müllertz, Y. Perrie & T. Rades (Eds.), *Analytical Techniques in the Pharmaceutical Sciences* (pp. 223-251). New York, NY: Springer New York.

Husband, H., Ferreira, S., Bu, F., Feyzi, S., & Ismail, B. P. (2024). Pea protein globulins: Does their relative ratio matter? *Food Hydrocolloids, 148*, 109429. https://doi.org/10.1016/j.foodhyd.2023.109429.

The Good Food Institute. (2023). Plant-based retail sales data for six European countries: 2022-2024. Retrieved from *https://gfieurope.org/european-plant-based-sales-data/.* Accessed May 14, 2025.

Jafarzadeh, S., Qazanfarzadeh, Z., Majzoobi, M., Sheiband, S., Oladzadabbasabad, N., Esmaeili, Y., Barrow, C. J., & Timms, W. (2024). Alternative proteins; A path to sustainable diets and environment. *Current Research in Food Science, 9*, 100882. https://doi.org/10.1016/j.crfs.2024.100882.

Kew, B., Holmes, M., Liamas, E., Ettelaie, R., Connell, S. D., Dini, D., & Sarkar, A. (2023). Transforming sustainable plant proteins into high performance lubricating microgels. *Nature Communications, 14*(1), 4743. https://doi.org/10.6084/m9.figshare.22722718.

Kew, B., Holmes, M., Stieger, M., & Sarkar, A. (2021). Oral tribology, adsorption and rheology of alternative food proteins. *Food Hydrocolloids, 116*, 106636. https://doi.org/10.1016/j.foodhyd.2021.106636.

Kim, J. T., Weber, N., Shin, G. H., Huang, Q., & Liu, S. X. (2007). The Study of β-Lactoglobulin Adsorption on Polyethersulfone Thin Film Surface Using QCM-D and AFM. *Journal of Food Science, 72*(4), E214-E221. https://doi.org/10.1111/j.1750-3841.2007.00344.x.

Klost, M., & Drusch, S. (2019). Functionalisation of pea protein by tryptic hydrolysis – Characterisation of interfacial and functional properties. *Food Hydrocolloids, 86*, 134-140. https://doi.org/10.1016/j.foodhyd.2018.03.013.

Kontturi, K. S., Tammelin, T., Johansson, L.-S., & Stenius, P. (2008). Adsorption of Cationic Starch on Cellulose Studied by QCM-D. *Langmuir, 24*(9), 4743-4749. https://doi.org/10.1021/la703604j.

Latypov, R. F., Liu, D., Gunasekaran, K., Harvey, T. S., Razinkov, V. I., & Raibekas, A. A. (2008). Structural and thermodynamic effects of ANS binding to human interleukin-1 receptor antagonist. *Protein Science, 17*(4), 652-663.https://doi.org/10.1110/ps.073332408.

Leermakers, F. A. M., Atkinson, P. J., Dickinson, E., & Horne, D. S. (1996). Self-Consistent-Field Modeling of Adsorbed β-Casein: Effects of pH and Ionic Strength on Surface Coverage and Density Profile. *Journal of Colloid and Interface Science, 178*(2), 681-693. https://doi.org/10.1006/jcis.1996.0166.

Lesme, H., Kew, B., Bonnet, L., Sarkar, A., & Stellacci, F. (2024). Difference in astringency of the main pea protein fractions. *Food Hydrocolloids, 149*, 109489. https://doi.org/10.1016/j.foodhyd.2023.109489.

Liamas, E., Connell, S. D., & Sarkar, A. (2023). Frictional behaviour of plant proteins in soft contacts: unveiling nanoscale mechanisms. *Nanoscale Advances, 5*(4), 1102-1114. https://doi.org/10.1039/D2NA00696K.

Liamas, E., Connell, S. D., Zembyla, M., Ettelaie, R., & Sarkar, A. (2021). Friction between soft contacts at nanoscale on uncoated and protein-coated surfaces. *Nanoscale, 13*(4), 2350-2367. https://doi.org/10.1039/D0NR06527G.

Lu, Z. X., He, J. F., Wang, Y. C., & Bing, D. J. (2020). Composition, physicochemical properties of pea protein and its application in functional foods. *Critical Reviews in Food Science and Nutrition, 60*(15), 2593-2605. https://doi.org/10.1080/10408398.2019.1651248.

Mariotti, F., Tomé, D., & Mirand, P. P. (2008). Converting nitrogen into protein--beyond 6.25 and Jones' factors. *Critical Reviews in Food Science and Nutrition, 48*(2), 177-184. https://doi.org/10.1080/10408390701279749.

Marquez Moreno, M. C., & Fernandez Cuadrado, V. (1993). Enzymic hydrolysis of vegetable proteins: mechanism and kinetics. *Process Biochemistry, 28*(7), 481-490. https://doi.org/10.1016/0032-9592(93)85032-B.

Meijers, M. G. J., Meinders, M. B. J., Vincken, J.-P., & Wierenga, P. A. (2023). Effect of Pea Legumin-to-Vicilin Ratio on the Protein Emulsifying Properties: Explanation in Terms of Protein Molecular and Interfacial Properties. *Journal of Agricultural and Food Chemistry, 71*(29), 11228-11238. https://doi.org/10.1021/acs.jafc.3c01589.

Mokni Ghribi, A., Maklouf Gafsi, I., Sila, A., Blecker, C., Danthine, S., Attia, H., Bougatef, A., & Besbes, S. (2015). Effects of enzymatic hydrolysis on conformational and functional properties of chickpea protein isolate. *Food Chemistry, 187*, 322-330. https://doi.org/10.1016/j.foodchem.2015.04.109.

Morell, P., López-García, A., Hernando, I., & Quiles, A. (2023). Improving Pea Protein Emulsifying Capacity by Glycosylation to Prepare High-Internal-Phase Emulsions. *Foods, 12*(4), 870. https://doi.org/10.3390/foods12040870.

Nikbakht Nasrabadi, M., Sedaghat Doost, A., & Mezzenga, R. (2021). Modification approaches of plant-based proteins to improve their techno-functionality and use in food products. *Food Hydrocolloids, 118*, 106789. https://doi.org/10.1016/j.foodhyd.2021.106789.

Plietz, P., Drescher, B., & Damaschun, G. (1987). Relationship between the amino acid sequence and the domain structure of the subunits of the 11S seed globulins. *International Journal of Biological Macromolecules, 9*(3), 161-165. https://doi.org/10.1016/0141-8130(87)90045-6.

Poore, J., & Nemecek, T. (2018). Reducing food's environmental impacts through producers and consumers. *Science, 360*(6392), 987-992. https://doi.org/10.1126/science.aaq0216.

Rubio, L. A., Pérez, A., Ruiz, R., Guzmán, M., Aranda-Olmedo, I., & Clemente, A. (2014). Characterization of pea (Pisum sativum) seed protein fractions. *Journal of the Science of Food and Agriculture, 94*(2), 280-287. https://doi.org/10.1002/jsfa.6250.

Scheutjens, J. M. H. M., & Fleer, G. J. (1979). Statistical theory of the adsorption of interacting chain molecules. 1. Partition function, segment density distribution, and adsorption isotherms. *The Journal of Physical Chemistry, 83*(12), 1619-1635. https://doi.org/10.1021/j100475a012.

Scheutjens, J. M. H. M., & Fleer, G. J. (1980). Statistical theory of the adsorption of interacting chain molecules. 2. Train, loop, and tail size distribution. *The Journal of Physical Chemistry, 84*(2), 178-190. https://doi.org/10.1021/j100439a011.

Shahbal, N., Jing, X., Bhandari, B., Dayananda, B., & Prakash, S. (2023). Effect of enzymatic hydrolysis on solubility and surface properties of pea, rice, hemp, and oat proteins: Implication on high protein concentrations. *Food Bioscience, 53*, 102515. https://doi.org/10.1016/j.fbio.2023.102515.

Shanthakumar, P., Klepacka, J., Bains, A., Chawla, P., Dhull, S. B., & Najda, A. (2022). The Current Situation of Pea Protein and Its Application in the Food Industry. *Molecules, 27*(16), 5354. https://doi.org/10.3390/molecules27165354.

Shuai, X., Gao, L., Geng, Q., Li, T., He, X., Chen, J., Liu, C., & Dai, T. (2022). Effects of Moderate Enzymatic Hydrolysis on Structure and Functional Properties of Pea Protein. *Foods, 11*(15), 2368. https://doi.org/10.3390/foods11152368.

Soltanahmadi, S., Murray, B. S., & Sarkar, A. (2022). Comparison of oral tribological performance of proteinaceous microgel systems with protein-polysaccharide combinations. *Food Hydrocolloids, 129*, 107660. https://doi.org/10.1016/j.foodhyd.2022.107660.

Stribițcaia, E., Gibbons, C., Finlayson, G., You, K.-M., Araiza-Calahorra, A., Hafiz, M. S., Ellis, L. R., Boesch, C., Sier, J. H., Blundell, J., & Sarkar, A. (2024). Effect of in vitro food oral coating and lubricity on satiety: A randomized controlled trial using milk protein beverages. *Physiology & Behavior, 287*, 114690. https://doi.org/10.1016/j.physbeh.2024.114690.

Surówka, K., Żmudziński, D., & Surówka, J. (2004). Enzymic modification of extruded soy protein concentrates as a method of obtaining new functional food components. *Trends in Food Science & Technology, 15*(3), 153-160. https://doi.org/10.1016/j.tifs.2003.09.013.

Tahir, A. B., Jiang, B., & Ali, K. (2024). Unraveling distinct potential of pea (Pisum sativum L.) fractions (legumin, vicilin and albumin) by structural and functional characterization. *Food Research International, 198*, 115332. https://doi.org/10.1016/j.foodres.2024.115332.

Teo, A., Dimartino, S., Lee, S. J., Goh, K. K. T., Wen, J., Oey, I., Ko, S., & Kwak, H.-S. (2016). Interfacial structures of whey protein isolate (WPI) and lactoferrin on hydrophobic surfaces in a model system monitored by quartz crystal microbalance with dissipation (QCM-D) and their formation on nanoemulsions. *Food Hydrocolloids, 56*, 150-160. https://doi.org/10.1016/j.foodhyd.2015.12.002.

Tian, Y., Qiu, M., Shen, Y., Zheng, Y., Yang, X., Zhang, W., & Jiang, Y. (2025). Interfacial properties of whey protein hydrolysates monitored by quartz crystal microbalance with dissipation. *International Journal of Biological Macromolecules, 301*, 140368. https://doi.org/10.1016/j.ijbiomac.2025.140368.

Venyaminov, S. Y., Baikalov, I. A., Shen, Z. M., Wu, C. S. C., & Yang, J. T. (1993). Circular Dichroic Analysis of Denatured Proteins: Inclusion of Denatured Proteins in the Reference Set. *Analytical Biochemistry, 214*(1), 17-24. https://doi.org/10.1006/abio.1993.1450.

Vlădescu, S.-C., Agurto, M. G., Myant, C., Boehm, M. W., Baier, S. K., Yakubov, G. E., Carpenter, G., & Reddyhoff, T. (2023). Protein-induced delubrication: How plant-based and dairy proteins affect mouthfeel. *Food Hydrocolloids, 134*, 107975. https://doi.org/10.1016/j.foodhyd.2022.107975.

Vogelsang-O'Dwyer, M., Sahin, A. W., Arendt, E. K., & Zannini, E. (2022). Enzymatic Hydrolysis of Pulse Proteins as a Tool to Improve Techno-Functional Properties. *Foods, 11*(9). https://doi.org/10.3390/foods11091307.

Wang, M., Ettelaie, R., & Sarkar, A. (2025). Enzymatic hydrolysis of legume proteins: lessons on surface property outcomes. *Current Opinion in Food Science, 62*, 101259. https://doi.org/10.1016/j.cofs.2024.101259.

Wang, Z., Zhang, L., Zhang, X., Zeng, M., He, Z., & Chen, J. (2021). Interfacial Rheology and Foaming Properties of Soy Protein and Hydrolysates under Acid Condition. *Food Biophysics, 16*(4), 484-491. https://doi.org/10.1007/s11483-021-09685-9.

Wooster, T. J., & Augustin, M. A. (2007). The emulsion flocculation stability of protein–carbohydrate diblock copolymers. *Journal of Colloid and Interface Science, 313*(2), 665-675. https://doi.org/10.1016/j.jcis.2007.04.054.

Wouters, A. G. B., Rombouts, I., Fierens, E., Brijs, K., & Delcour, J. A. (2016). Relevance of the Functional Properties of Enzymatic Plant Protein Hydrolysates in Food Systems. *Comprehensive Reviews in Food Science and Food Safety, 15*(4), 786-800. https://doi.org/10.1111/1541-4337.12209.

Xu, F., Liamas, E., Bryant, M., Adedeji, A. F., Andablo-Reyes, E., Castronovo, M., Ettelaie, R., Charpentier, T. V. J., & Sarkar, A. (2020). A Self-Assembled Binary Protein Model Explains High-Performance Salivary Lubrication from Macro to Nanoscale. *Advanced Materials Interfaces, 7*(1), 1901549. https://doi.org/10.1002/admi.201901549.

Yang, J., Huang, F., Huang, Q., Ma, D., Chen, Y., Peng, D., Yu, X., Deng, Q., & Geng, F. (2023). Physical and emulsifying properties of pea protein: influence of combined physical modification by flaxseed gum and ultrasonic treatment. *Food Science and Human Wellness, 12(2), 431-441.* https://doi.org/10.1016/j.fshw.2022.07.045

Yang, J., Mocking-Bode, H. C. M., van den Hoek, I. A. F., Theunissen, M., Voudouris, P., Meinders, M. B. J., & Sagis, L. M. C. (2022). The impact of heating and freeze or spray drying on the interface and foam stabilising properties of pea protein extracts: Explained by aggregation and protein composition. Food Hydrocolloids, 133, 107913. https://doi.org/10.1016/j.foodhyd.2022.107913.

Yang, T., Zan, S., Li, B., Li, L., & Zhang, X. (2024). Interfacial adsorption dynamics of solid lipid particles at oil/water interfaces through QCM-D technique. *Food Hydrocolloids, 148*, 109431. https://doi.org/10.1016/j.foodhyd.2023.109431.

Yang, Z., Dai, L., Sun, Q., McClements, D. J., & Xu, X. (2022). Effect of molecular weight on the interfacial and emulsifying characteristics of rice glutelin hydrolysates. *Food Hydrocolloids, 128*, 107560. https://doi.org/10.1016/j.foodhyd.2022.107560.

Zembyla, M., Liamas, E., Andablo-Reyes, E., Gu, K., Krop, E. M., Kew, B., & Sarkar, A. (2021). Surface adsorption and lubrication properties of plant and dairy proteins: A comparative study. *Food Hydrocolloids, 111*, 106364. https://doi.org/10.1016/j.foodhyd.2020.106364.

Zhang, A., Li, X., Liu, B., Yin, Y., Zhang, H., & Zhang, Y. (2023). Comprehensive application possibility: Construction hydrophilic, amphiphilic and hydrophobic system of modified zein by enzymatic or cysteine modification. *Food Hydrocolloids, 135*, 108159. https://doi.org/10.1016/j.foodhyd.2022.108159.

Zhang, Y., & Romero, H. M. (2020). Exploring the structure-function relationship of Great Northern and navy bean (Phaseolus vulgaris L.) protein hydrolysates: A study on the effect of enzymatic hydrolysis. *International Journal of Biological Macromolecules, 162*, 1516-1525. https://doi.org/10.1016/j.ijbiomac.2020.08.019.

Figures

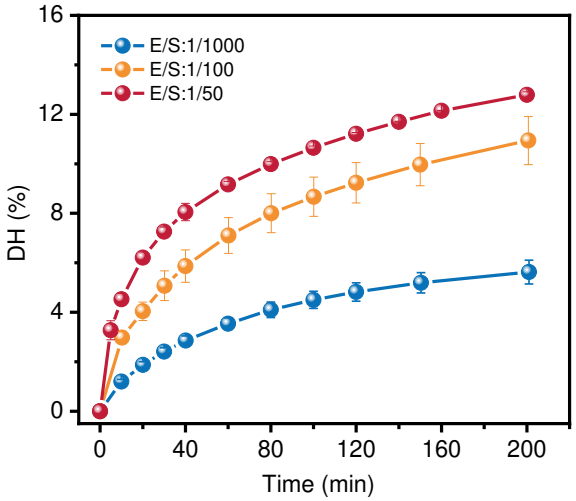

Figure 1. Experimental degree of hydrolysis (%DH) of the 11S legumin-rich fraction (LR) as a function of time measured using the pH-stat method, with different enzyme-to-substrate ratios (E/S) of 1:50, 1:100, and 1:1000 w/w. Data are presented as means and standard deviations for at least duplicate samples (n = 2 × 2).

(a)

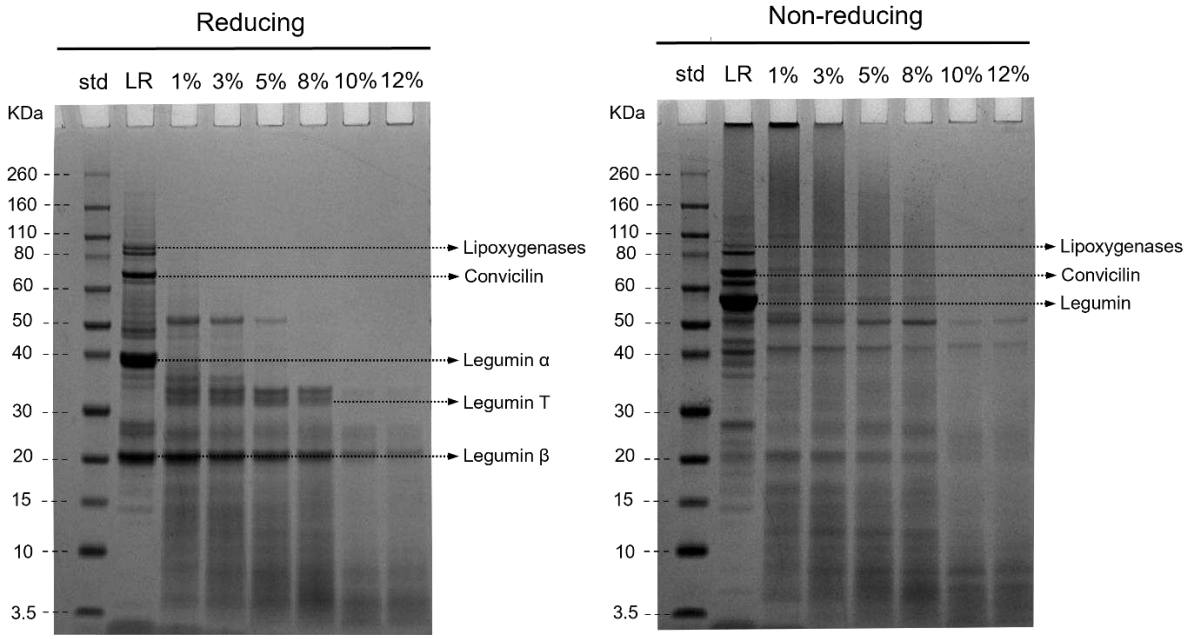

(b)

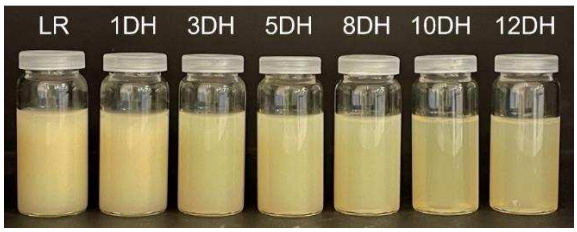

Figure 2. Sodium dodecyl-sulfate polyacrylamide gel electrophoresis (SDS-PAGE) (a) of various trypsin-hydrolyzed samples with %DH ranging from 1% to 12% under reducing (left) and non-reducing (right) conditions. In both gels (a), lanes from the left to right correspond to the molecular weight standard, unhydrolyzed LR and hydrolysates at 1%DH, 3%DH, 5%DH, 8%DH, 10%DH and 12%DH. (b) The visual appearance of 2% (w/v) LR and its hydrolysates with varying %DH levels are shown at pH 7.0.

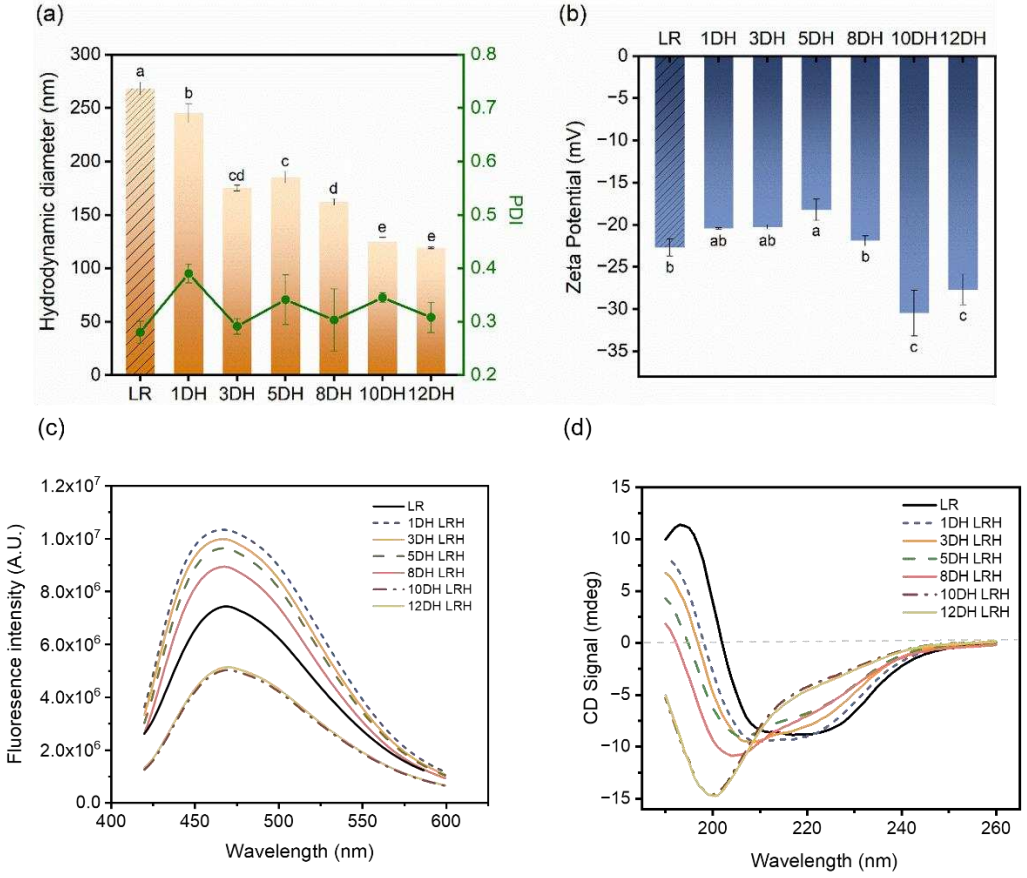

Figure 3. Mean hydrodynamic diameter (d_H) and polydispersity index (PDI) (a), ζ-potential (b), surface hydrophobicity (c) and Far-UV Circular Dichroism (CD) spectra (d) of LR dispersion and its hydrolysates at pH 7.0. The CD signal shown in Figure 4(d) has been

normalized to the signal derived from PBS buffer to get rid of the background influence. Data are represented as means and standard deviations for at least two independent samples (n = 2 x 3). Samples with the same letters indicate no significant difference ($p > 0.05$) as determined by Tukey's test.

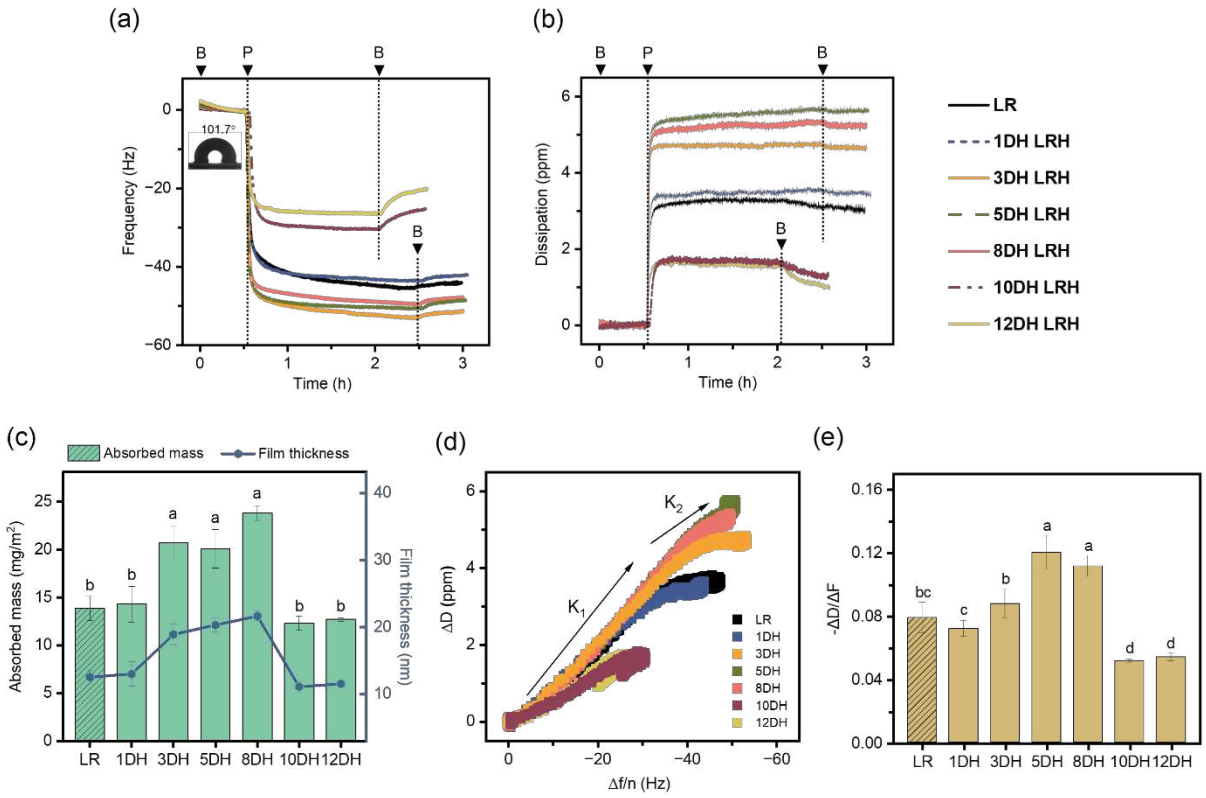

Figure 4. Normalized frequency shift (a), dissipation shift (b) as a function of time (obtained from the 5th overtone of the QCM-D measurement), mean hydrated mass and film thickness (c), normalized ΔD as a function of Δf (d), film viscoelasticity (-ΔD/Δf) (e) of LR and its hydrolysate dispersions at pH 7.0. In Figures 4(a) and (b), the baseline was established using a buffer solution (B), after which 0.01% (w/v) LR/ hydrolysate (with 1%~12%DH) dispersions at pH 7.0 were added to facilitate protein adsorption (P) on the bare PDMS-coated sensor surface. This was followed by a washing step using buffer solution to remove the loosely adsorbed proteins/ hydrolysates. Steps B and P in the figures indicate the onset of buffer rinsing and protein addition, respectively. The inserted contact angle image in Figure 4(a) shows the hydrophobic property of used bare PDMS-coated sensors when exposed to PBS solution. In Figure 4(d), the real-time conformational changes of the formed protein film for the adsorption stage were depicted as two stages of adsorption kinetics, denoted as K_1 and K_2. All data in Figures 4(c) and 4(d) were presented as means with standard deviations, shown as error bars. Samples with the same letters represent insignificant difference ($p > 0.05$) according to Tukey's test

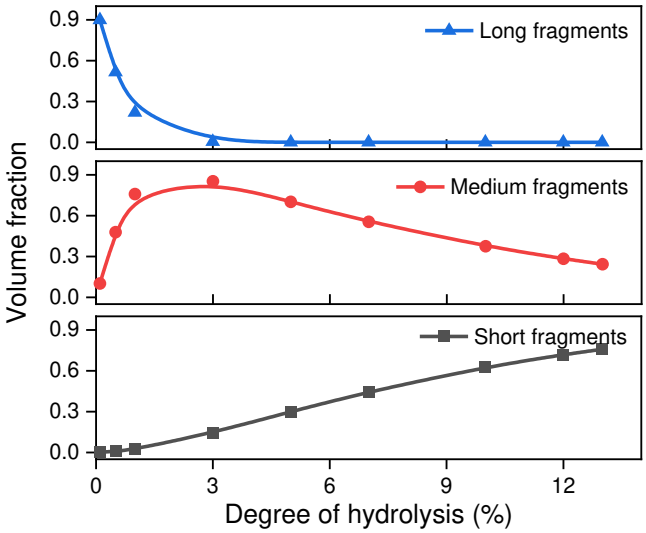

1053

1054 **Figure 5.** Calculated relative volume fraction of long (N=222-517), medium (N=21-221),
1055 and short (N<20) fragment populations as a function of degree of hydrolysis (%DHs). In
1056 each population, the volume fraction contributions of all potential fragments were added.

1057

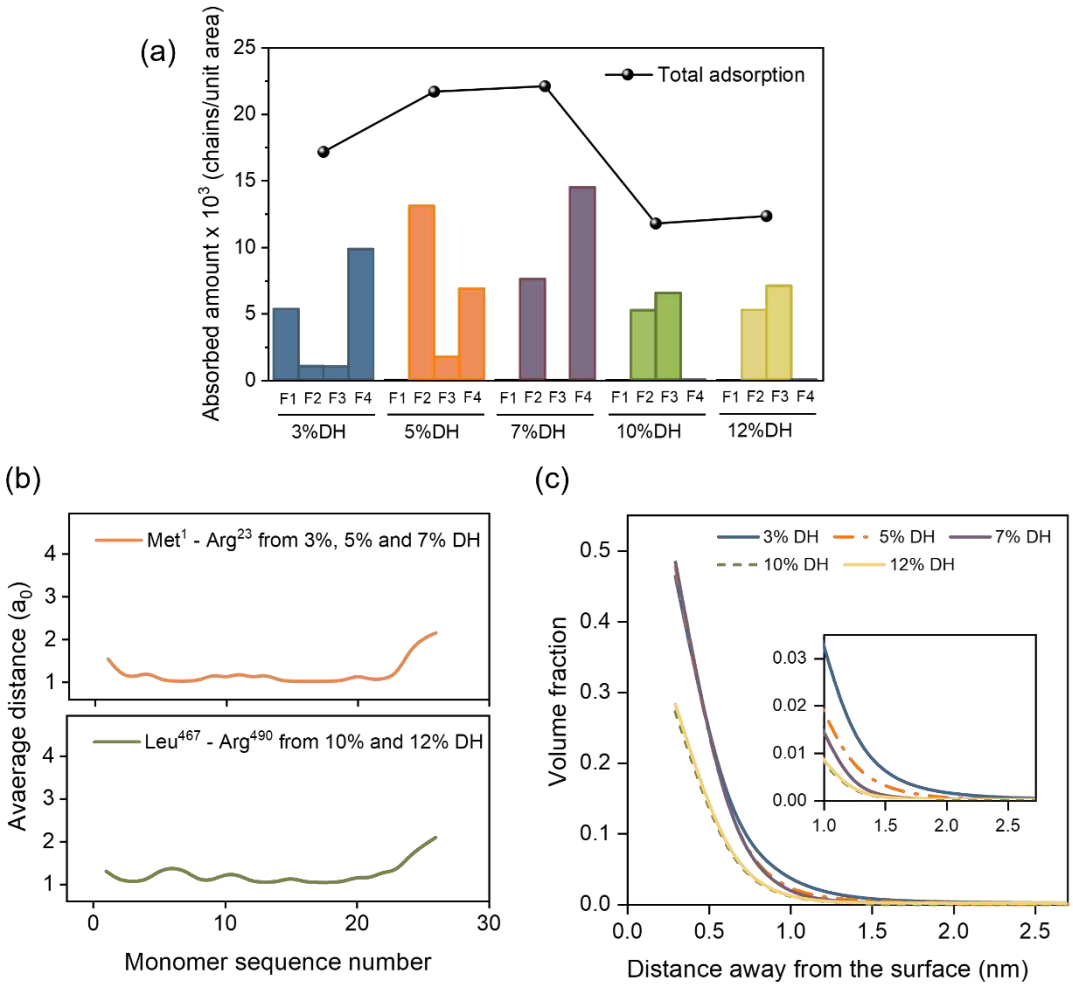

Figure 6. Absorbed quantities of individual fragments (F1, F2, F3 and F4) as well as the total adsorbed chains (a) calculated from SCF calculations under different %DH values. Total adsorption (Γ_{total}, shown as the grey line) represents the sum of Γ of four considered fragments (Γ_{F1}, Γ_{F2}, Γ_{F3}, Γ_{F4}) that are close to the hydrophobic surface. Predicted configuration (b) of the dominant fragment absorbed on a hydrophobic surface. Under each %DH situation, the surface-dominant fragment varies, as displayed in Figure 6a, namely Met ^{1} – Arg ^{23} at 3%, 5% and 7% DH, respectively, Leu ^{467} – Arg ^{490} at 10% and 12% DH, respectively. Their corresponding protein sequence can be sourced from Figure S1. Density profile (c) of the four-fragment mixture. The total volume fraction variation (*i.e.* $\Phi_{F1}+\Phi_{F2}+\Phi_{F3}+\Phi_{F4}$) is plotted against the distance away from the hydrophobic surface. The insert graph provides a magnified view of the region of interest. All calculations were conducted at a background electrolyte volume fraction of 0.001 (~10 mM NaCl) and at a solution pH of 7.0.

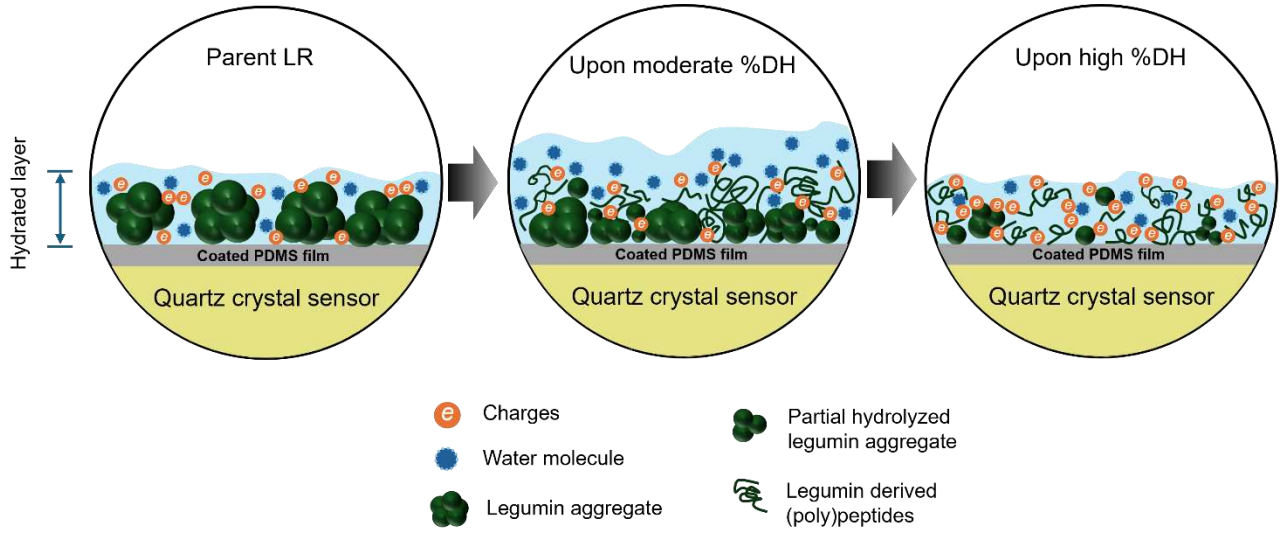

1073

1074 **Figure 7**. Schematic diagram of LR surface adsorption as a function of various %DHs.

1075

1076

Supplementary Information

Surface adsorption of legume proteins upon tryptic hydrolysis: Theoretical and experimental study

Mingxin Wang [1], Rammile Ettelaie [1*] and Anwesha Sarkar [1,2 *]

[1] Food Colloids and Bioprocessing Group, School of Food Science and Nutrition, University of Leeds, Leeds, LS2 9JT, UK

[2] National Alternative Protein Innovation Centre (NAPIC), UK

Corresponding authors:

*Prof. Anwesha Sarkar

E-mail address: A.Sarkar@leeds.ac.uk

*Dr. Rammile Ettelaie

E-mail address: r.ettelaie@leeds.ac.uk

Table S1. Calculated total net charge of the four-fragment constituting mixtures generated at different %DHs at pH 7.0, based on the pKa value of each AA component.

	3 %DH	5 %DH	7 %DH	10 %DH	12 %DH
Net charge/ e	–4.95	–8.94	–8.95	–11.22	–11.22

Self-consistent field theory

In the designed 3D lattice grid, every lattice site is occupied by any one of a monomer amino acid (AA), an ion, or a solvent molecule with no site remaining empty. Each site is only able to accommodate one such monomer or molecule. Defined in this way, this setup implies that the volume fraction of each species equals to its number density in a layer. Hence, the essential calculation in SCF is the most probable density profile for each specie in the gap. Strictly speaking, the thermodynamic quantities of interest should be averaged over all the possible density profile variations, each weighted with their own likelihood of occurrence, as determined by the appropriate Boltzmann factor $\sim \exp\left(-\frac{F\left(\left\{\varphi_i^{\alpha(r)}\right\}\right)}{k_B T}\right)$, where $F\left(\left\{\varphi_i^{\alpha(r)}\right\}\right)$ is the free energy of molecules adapting a density profile variation across the gap $\left\{\varphi_i^{\alpha(r)}\right\}$. For a protein, existing between two approaching flat plates, in equilibrium with bulk solution outside the gap, the free energy functional per unit area of the system is (Ettelaie, et al., 2008):

$$\frac{\Delta F}{k_{\mathrm{B}}T} = -\int_0^L \left[\sum_i \frac{1}{N_i}\sum_\alpha (\Phi_i^\alpha(r) - \Phi_i^\alpha)\right] dr - \int_0^L \left[\sum_\alpha \psi_\alpha(r) \sum_i \Phi_i^\alpha(r)\right] dr$$

$$+\frac{1}{2}\int_0^L \left[\sum_{i,j}\sum_{\alpha\neq\beta} \chi_{\alpha\beta}(\Phi_i^\alpha(r) - \Phi_{\mathrm{i}}^\alpha)\,(\Phi_j^\beta(r) - \Phi_j^\beta)\right] dr$$

$$+\frac{1}{2}\int_0^L \left[\psi_e(r)\sum_\alpha q_\alpha \sum_i \Phi_i^\alpha(r)\right] dr + \sum_\alpha \chi_{\alpha s}\sum_i [\Phi_i^\alpha(0) + \Phi_i^\alpha(L)]$$

(S1)

where, *L* represents the space between two planar surfaces, and r denotes the distance away from one of the surfaces *i.e.* 0 < *r* < *L*. The variation of the density profile of type α AA residues belonging to chain i across the gap is denoted as $\Phi_i^\alpha(r)$, where N_i is the total number of the AA residues making up the chain i. When those α type AA residues are sufficiently far away from the surface, not being influenced at all by the presence of the surface, $\Phi_i^\alpha(r)$ is indicated as Φ_i^α. which also implies that the prespecified bulk volume fraction of AA residues belonging to the considered protein i is Φ_i^α. The symbols k_B and *T* denote the Boltzmann constant and temperature, respectively.

Table S2. Categorisation of involved amino acid residues in Legumin A.

Category number	Properties	Including amino acid residues
1	Hydrophobic	Pro, Ile, Gly, Leu, Val, Phe, Ala, Met, Trp
2	Polar (non-charged)	Gln, Asn, Ser, Thr, Cys, Tyr
3	Positive charged	Arg, Lys, N-terminus
4	Special positive charged	His [a]
5	Negative charged	Glu, Asp, C-terminus

a. Histidine (His) is classified in a group of its own (in Category 5) and not with other positively charged AAs, as its unique pKa compared to others makes it difficult to place them together.

Table S3. Composition and length of the four most dominant fragments as represented by their volume fractions, at various %DH produced by trypsin.

	Most dominant fragment (F1)	**Second dominant fragment (F2)**	**Third dominant fragment (F3)**	**Fourth dominant fragment (F4)**
3 %DH	Met ^{1} – Lys ^{60}	Met ^{1} – Arg ^{35}	Met ^{1} – Arg ^{44}	Met ^{1} – Arg ^{23}
5 %DH	Pre ^{82} – Arg ^{123}	Met ^{1} – Arg ^{23}	Met ^{1} – Arg ^{35}	Glu ^{137} – Arg ^{168}
7 %DH	Pre ^{82} – Arg ^{123}	Glu ^{137} – Arg ^{168}	Leu ^{467} – Arg ^{490}	Met ^{1} – Arg ^{23}
10 %DH	Pre ^{82} – Arg ^{123}	Glu ^{137} – Arg ^{168}	Leu ^{467} – Arg ^{490}	Phe ^{181} – Lys ^{201}
12 %DH	Pre ^{82} – Arg ^{123}	Glu ^{137} – Arg ^{168}	Leu ^{467} – Arg ^{490}	Phe ^{181} – Lys ^{201}

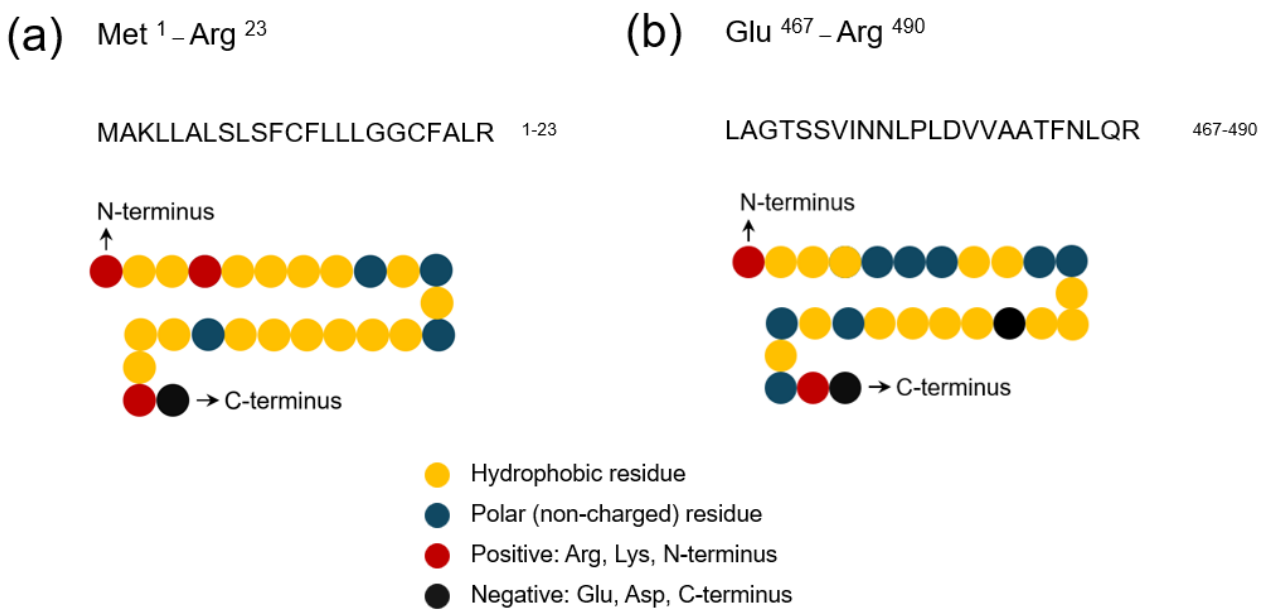

Figure S1. The amino acid sequence of fragment Met ^{1} – Arg ^{23} (a) and Leu ^{467} – Arg ^{490} (b) with the component amino acids grouped as indicated. The sequences were sourced from UniProt database.

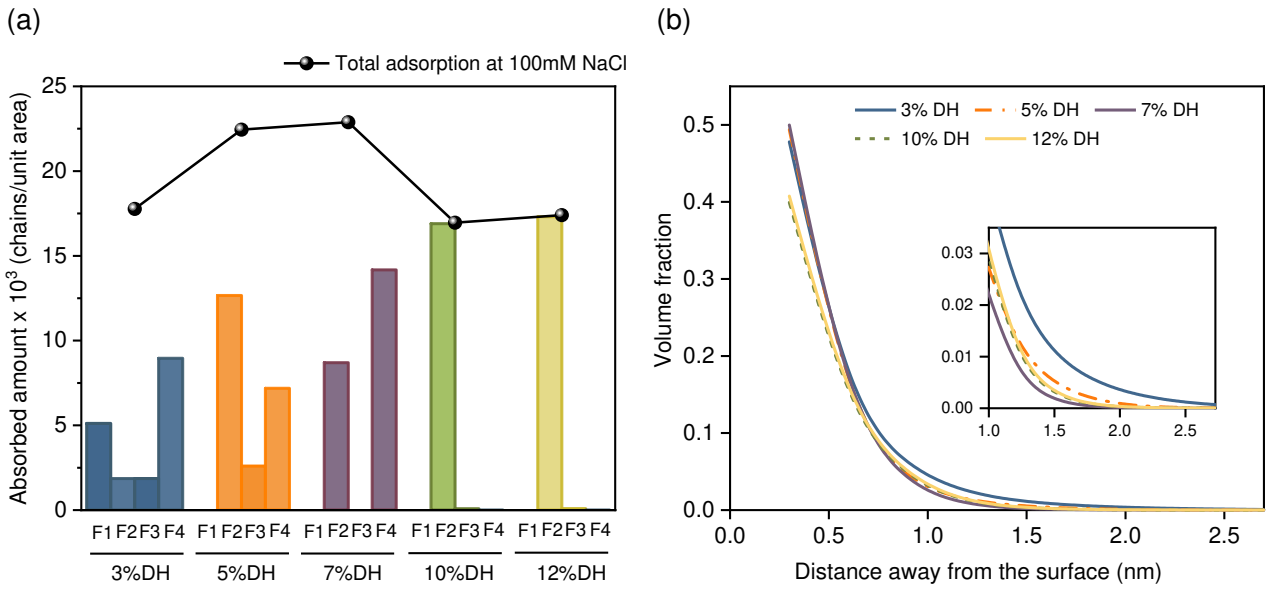

Figure S2. Absorbed quantities (a) of individual fragments (F1, F2, F3 and F4) as well as the total adsorbed chains calculated from SCF calculations. Total adsorption (Γ_{total}, shown as the grey line) represents the sum of Γ of four considered fragments (Γ_{F1}, Γ_{F2}, Γ_{F3}, Γ_{F4}) that are close to the hydrophobic surface. Density profile (b) of the four- fragment mixture. The total volume fraction variation (*i.e.* $\Phi_{F1}+\Phi_{F2}+\Phi_{F3}+\Phi_{F4}$) is plotted against the distance away from the hydrophobic surface. All calculations involved in (a) and (b) were conducted at a background electrolyte volume fraction of 0.01 (~100 mM NaCl) and at a solution pH of 7.0.

Kevin-Voigt Model applied to calculate hydrated mass and film thickness using QCM-D

Globular proteins are generally considered to form a hydrated surface layer rather than a stiff one. Hence, a viscoelastic model—Kevin-Voigt model was applied to quantify protein surface adsorption. In QCM-D analysis, the raw frequency and dissipation data was further fitted with this model to obtain the hydrated mass adsorption and film thickness. The fitting equation can be described as (Liu & Kim, 2009; Voinova, Rodahl, Jonson, & Kasemo, 1999):

$$\Delta f \approx -\frac{1}{2\pi\rho_0 h_0}\left\{\frac{\eta_2}{\delta_2} + h_1\rho_1\omega - 2h_1\left(\frac{\eta_2}{\delta_2}\right)^2\frac{\eta_1\omega^2}{\mu_1^2+\omega^2\eta_1^2}\right\} \quad \text{(S2)}$$

$$\Delta D \approx \frac{1}{\pi f\rho_0 h_0}\left\{\frac{\eta_2}{\delta_2} + 2h_1\left(\frac{\eta_2}{\delta_2}\right)^2\frac{\eta_1\omega}{\mu_1^2+\omega^2\eta_1^2}\right\} \quad \text{(S3)}$$

Where ρ_0 and h_0 are the density and thickness of the quartz crystal. η_2 is the viscosity of the bulk liquid and δ_2 is the viscous penetration depth of the acoustical vibrations through the absorbed layer in the bulk liquid and ρ_3 is the density of bulk liquid. ω is the angular frequency of the oscillation. The properties of the adsorbed layer were described by its density (ρ_1), viscosity (η_2), shear elasticity (μ_1), and thickness (δ_1). The thickness of the absorbed layer (h_1) was obtained by dividing the hydrated mass by the layer density, which was assumed to be 1100 kg/m^3 for the hydrated protein layer in this study.

References

Ettelaie, R., Akinshina, A., & Dickinson, E. (2008). Mixed protein–polysaccharide interfacial layers: a self consistent field calculation study. *Faraday Discussions, 139*(0), 161-178.https://doi.org/10.1039/B717199D.

Liu, S. X., & Kim, J.-T. (2009). Application of Kevin—Voigt Model in Quantifying Whey Protein Adsorption on Polyethersulfone Using QCM-D. *SLAS Technology, 14*(4), 213-220. https://doi.org/10.1016/j.jala.2009.01.003.

Voinova, M. V., Rodahl, M., Jonson, M., & Kasemo, B. (1999). Viscoelastic Acoustic Response of Layered Polymer Films at Fluid-Solid Interfaces: Continuum Mechanics Approach. *Physica Scripta, 59*(5), 391. https://doi.org/10.1238/Physica.Regular.059a00391.